DEVELOPMENTAL NEUROSCIENCE

Nzf2 promotes oligodendrocyte differentiation and regeneration via repressing HDAC1-mediated histone deacetylation

Xiaofeng Xu[1], Minxi Fang[1,2], Lixia Chen[1], Hao Huang[1], Zhong-Min Dai[1], Junlin Yang[1], Mengsheng Qiu[1]*

Proper axonal myelination and function of the vertebrate central nervous system rely largely on the timely differentiation of oligodendrocytes (OLs), yet key regulatory factors remain enigmatic. Our study reveals neural zinc finger (Nzf2) as a crucial orchestrator that controls the timing of OL differentiation both during development and myelin repair, contrasting with its previously suggested role in direct myelin gene regulation. *Nzf2* ablation delays the onset of OL differentiation, while hyperactivation stimulates OL differentiation both during development and remyelination. Using RNA-seq and ChIP-seq, we pinpoint Nkx2.2 as a critical downstream target of Nzf2. Specific binding of Nzf2 in the *Nkx2.2* gene locus inhibits histone deacetylation by disrupting the HDAC1 repressor complex and reducing deacetylase activity. Furthermore, Nzf2 overrides the inhibitory Notch signaling to initiate OL differentiation. Thus, we propose that the Notch-Nzf2-Nkx2.2 axis is a vital component of OL differentiation timing mechanism, suggesting Nzf2 as a potential therapeutic target for stimulating OL differentiation and boosting myelin repair in demyelinating diseases.

INTRODUCTION

Oligodendrocytes (OLs) produce myelin sheaths that electrically insulate axons and promote rapid propagation of action potential in the central nervous system (CNS). During myelination, the OL lineage goes through multiple developmental stages, including oligodendrocyte progenitor cells (OPCs), newly formed OLs (NFOs), and mature myelinating OLs (MOLs) (*1*). Single-cell RNA transcriptomic analyses recently identified a critical intermediate OL population between OPCs and NFOs, called differentiated-committed OPCs (COPs) (*2*, *3*). Defective myelinogenesis has been implicated in cognitive deficits and motor learning (*4*, *5*). Failure of OLs to remyelinate demyelinated axons leads to irreversible axonal degeneration in demyelinated diseases [e.g., multiple sclerosis (MS) and leukodystrophies] (*6*, *7*). The observation that OPCs are present within demyelinated lesions in MS but fail to differentiate into MOLs suggests that induction or initiation of OPC differentiation is a critical event for successful remyelination (*8*–*12*). Exploration of the timing control of OL differentiation during development will help us better understand the myelination/remyelination process and discover potential therapeutic targets for CNS myelin repair.

Temporal control of OL differentiation is essential for proper axonal myelination and function of vertebrate CNS (*13*–*15*). Although several regulatory factors for OL lineage progression and myelin elaboration, including Olig1/Olig2 (*16*, *17*), SRY-box transcription factor 10 (Sox10) (*18*), and myelin regulatory factor (Myrf) (*19*), have been characterized, our understanding of the timing mechanism of OL differentiation remains limited. Increasing evidences indicate that Nk2 homeobox 2 (Nkx2.2) is a key timing component of OL differentiation. Our previous work demonstrated that Nkx2.2 expression is up-regulated in differentiating OPCs (*20*, *21*), and disruption of Nkx2.2 leads to a marked delay of OL differentiation and myelin production (*22*). In addition, Notch signaling has been implicated in regulating the timing of OL differentiation (*23*), as blocking Notch signaling in OPCs results in robust precocious OL differentiation during development (*24*). However, the genetic interactions among these timing factors are not conspicuous, and additional intermediate factors are likely to be involved.

In this study, through single-cell RNA sequencing (scRNA-seq) analyses of the developing spinal tissues, we uncovered the neural zinc finger protein Nzf2, also referred to as myelin transcription factor 1 (Myt1) (*25*–*27*), as a major cell-intrinsic switch that drives OL differentiation. In support, misexpression of Nzf2 in immature OPCs can alter the timing of OL differentiation both in vivo and in vitro. Nzf2 substantially increases remyelination in a focal demyelination model. Mechanistically, we discovered that Nzf2 inhibits the nucleosomal histone deacetylation of the target gene *Nkx2.2*, via hindering the assembly of histone deacetylase 1 (HDAC1) repressor complexes, thus establishing an active chromatin landscape and promoting Nkx2.2 expression. In addition, our studies also demonstrated that Nzf2 expression is repressed by upstream Notch signaling in immature OPCs. Collectively, our findings have provided the compelling molecular and genetic evidence that the Notch-Nzf2-Nkx2.2 axis controls the onset of OL differentiation and myelin development, pointing to a potential strategy for enhancing CNS myelin regeneration.

RESULTS

Nzf2 is selectively up-regulated in late OPCs and differentiated OLs

Timely differentiation of OLs is crucial for ensuring proper myelination during CNS development. To comprehensively identify the key regulatory factors involved in initiating OL differentiation, we conducted scRNA-seq analyses on mouse spinal cord tissues isolated at embryonic day 15.5 (E15.5) and postnatal day 4 (P4) and P15, when OLs undergo active differentiation and myelination. Among the

[1]Zhejiang Key Laboratory of Organ Development and Regeneration, College of Life and Environmental Sciences, Hangzhou Normal University, Hangzhou 311121, China. [2]College of Life Sciences, Zhejiang University, Hangzhou 310058, China. *Corresponding author. Email: msqiu@hznu.edu.cn

30,511 single cells captured and sequenced, a total of 9031 cells were classified as belonging to the OL lineage based on further gene expression analysis. Using Uniform Manifold Approximation and Projection (UMAP) for cellular dimensionality reduction, we delineated the developmental trajectory of OL lineage cells, spanning from OPCs to MOLs (Fig. 1A). Our scRNA-seq analysis revealed that Nzf2 is highly expressed in OPCs and COPs, but its expression is reduced in NFOs and is minimal or undetectable in MOLs (Fig. 1B). Upon further subclassification of early postnatal OL lineage cells based on the criteria established by Marques *et al.* (*28*), we observed that Nzf2 is specifically expressed in all subclasses of OPCs and COPs (fig. S1, A and B).

To verify the selective expression of Nzf2 in differentiating OPCs, we generated a Nzf2-specific antibody corresponding to a unique sequence located between the acidic region and CCHC zinc fingers (fig. S1C). Starting at E15.5, a nuclear Nzf2 signal was detected in migrating cells within the basolateral mantle zone, a region characteristic of OPCs (Fig. 1C). Double immunostaining experiments further revealed that Nzf2 colocalized with the pan-oligodendroglial marker Sox10 (Fig. 1D, a, d, and g). Upon the initiation of OL differentiation in the white matter after birth, Nzf2 was detected in COPs and NFOs, which were identified by G protein-coupled receptor 17 (GPR17), Myrf, and CC1 immunoactivity, respectively (Fig. 1D, b, c, e, and f). The expression of Nzf2 in oligodendroglial cells peaked at P7 and gradually declined thereafter (Fig. 1D, g and h). Consequently, the proportion of $Nzf2^+$ cells among Sox10 or $CC1^+$ cells steadily decreased after birth (Fig. 1E). At P15, approximately 12% of $CC1^+$ cells exhibited Nzf2 staining (Fig. 1E). Additional analysis demonstrated that Nzf2 was not expressed in Aspartoacylase+ (ASPA+) mature OLs (Fig. 1D, i), which is in agreement with the scRNA-seq data showing minimal *Nzf2* transcript levels in these cells (Fig. 1B). Expression analysis in the developing forebrain also corroborated the specific expression of Nzf2 in $Olig2^+$, $Sox10^+$, and $CC1^+$ late OPCs or NFOs (fig. S1D). Collectively, these findings indicate that Nzf2 is robustly but transiently up-regulated in late OPCs, COPs, and NFOs (Fig. 1F), implying a crucial role for Nzf2 in initiating OPC differentiation, rather than in the morphological maturation or axonal myelination following differentiation.

Notably, the Nzf2 signal was also colocalized with the pan-neuronal marker NeuN in the gray matter (fig. S1E, a to c), but not with the astrocyte marker glial fibrillary acidic protein (GFAP; fig. S1E, d to f). Contrary to its dynamic expression pattern observed in the OL lineage, Nzf2 exhibits stable and sustained expression in developing neurons (fig. S1F), in keeping with the previous findings that Nzf2 could influence neuronal differentiation (*29*).

Ablation of *Nzf2* leads to a marked delay in the initiation of OL differentiation

To gain insight into the in vivo function of Nzf2 in oligodendrogenesis, we examined the expression of various stage-specific oligodendroglial markers in conventional *Nzf2* knockout (KO) mice (*30*). Homozygous mutant ($Nzf2^{-/-}$) mice died immediately after birth and exhibited no overt anomalies (fig. S2A). Through immunostaining and Western blotting analyses of spinal cord and brain tissues, we confirmed the absence of Nzf2 protein in $Nzf2^{-/-}$ mice at P0 [Fig. 2, A (b) and B]. To investigate OL differentiation in *Nzf2* mutants, we assessed the expression of several myelin genes. Both immunostaining and RNA in situ hybridization (ISH) revealed that the expression of Myrf, *Mbp*, or *Plp1* was undetectable in the spinal tissues of $Nzf2^{-/-}$ mice at P0 [Fig. 2, A (d, f, and h) and C], contrary to their robust expression in the white matter of control mice (Fig. 2A, c, e, and g). This inhibition of OL differentiation was also evident in the developing brain. At birth, numerous Mbp^+ or $Plp1^+$ OLs were detected in the ventral hindbrain of control mice (Fig. 2D, a and c) but none in $Nzf2^{-/-}$ mice [Fig. 2, D (b and d) and E]. Unfortunately, because of the neonatal lethality of $Nzf2^{-/-}$ mice, further assessment of OL development in the postnatal period was not feasible.

There are two plausible explanations for the absence of myelin gene expression in $Nzf2^{-/-}$ mice. One possibility is that OL differentiation merely experiences a delay in the absence of Nzf2 activity. Alternatively, a Nzf2 function is absolutely required for the terminal differentiation of OLs. To distinguish between these two scenarios, thoracic spinal cord explants were isolated from E14.5 control and $Nzf2^{-/-}$ mice and subsequently cultured on polycarbonate membranes in vitro. After 7 days of suspension culture (equivalent to P3 in vivo), whole-mount RNA in situ hybridization detected a substantial number of Mbp^+ cells in both control and $Nzf2^{-/-}$ tissues (Fig. 2F). However, it is noteworthy that the number of these cells remained comparatively lower in the mutant tissues (Fig. 2G). To further explore the direct impact of Nzf2 deficiency on oligodendroglial cells, we generated $Olig1^{cre}$; $Nzf2^{fx/fx}$ conditional knockout (cKO) mice in which Nzf2 is specifically ablated in OPCs (fig. S2, B and C). In line with the findings from the spinal cord explant experiments, the expression of *Mbp*, *Plp1*, and Myrf was notably diminished in the spinal cords of *Nzf2* cKO mice at P3, while the expression of Sox10 remained comparable between the controls and mutants (fig. S2, C and D). These results strongly suggested that the absence of OLs in *Nzf2* mutants was caused by delayed differentiation of OPCs rather than a defective differentiation program.

To eliminate the notion that the delayed OL differentiation observed in *Nzf2* mutants could be attributed to a scarcity of OPCs, we assessed the generation and proliferation of OPCs in spinal tissues. At E12.5, immediately following the initiation of OPC specification, no apparent alterations were detected in the generation and migration of $Olig2^+$ cells between the spinal cords of control and $Nzf2^{-/-}$ mice (fig. S2E). Moreover, the quantity and distribution of $Pdgfr\alpha^+$ and $Olig2^+$ OPCs remained comparable at subsequent embryonic stages (fig. S2, E and F), arguing that Nzf2 was not essential for OPC specification, migration, and proliferation. At P0, the number of $Olig2^+$, $Sox10^+$, and $Pdgfr\alpha^+$ cells was slightly but substantially elevated in $Nzf2^{-/-}$ mice, potentially due to an accumulation of undifferentiated OPCs (Fig. 2, H and I). Dual immunostaining with Sox10 and proliferation markers Ki67 and cyclin D1 revealed comparable results between $Nzf2^{-/-}$ and control littermates, implying similar rates of OPC proliferation in both genotypes (Fig. 2, J and K). In addition, no impact on cell survival was observed, as evidenced by the comparable number of active caspase 3–positive cells at P0 (fig. S2, G and H). Collectively, these findings suggest that early oligodendroglial development in $Nzf2^{-/-}$ mice proceeded normally during embryogenesis until the onset of OPC differentiation at the neonatal stage.

Hyperactivation of Nzf2 induces precocious OL differentiation both in vitro and in vivo

To investigate whether Nzf2 autonomously regulates OL differentiation, we overexpressed Nzf2 in the CG4 oligodendroglial cell line and analyzed its effect on cell differentiation. Lentiviruses expressing the doxycycline hydrochloride (Dox)–inducible

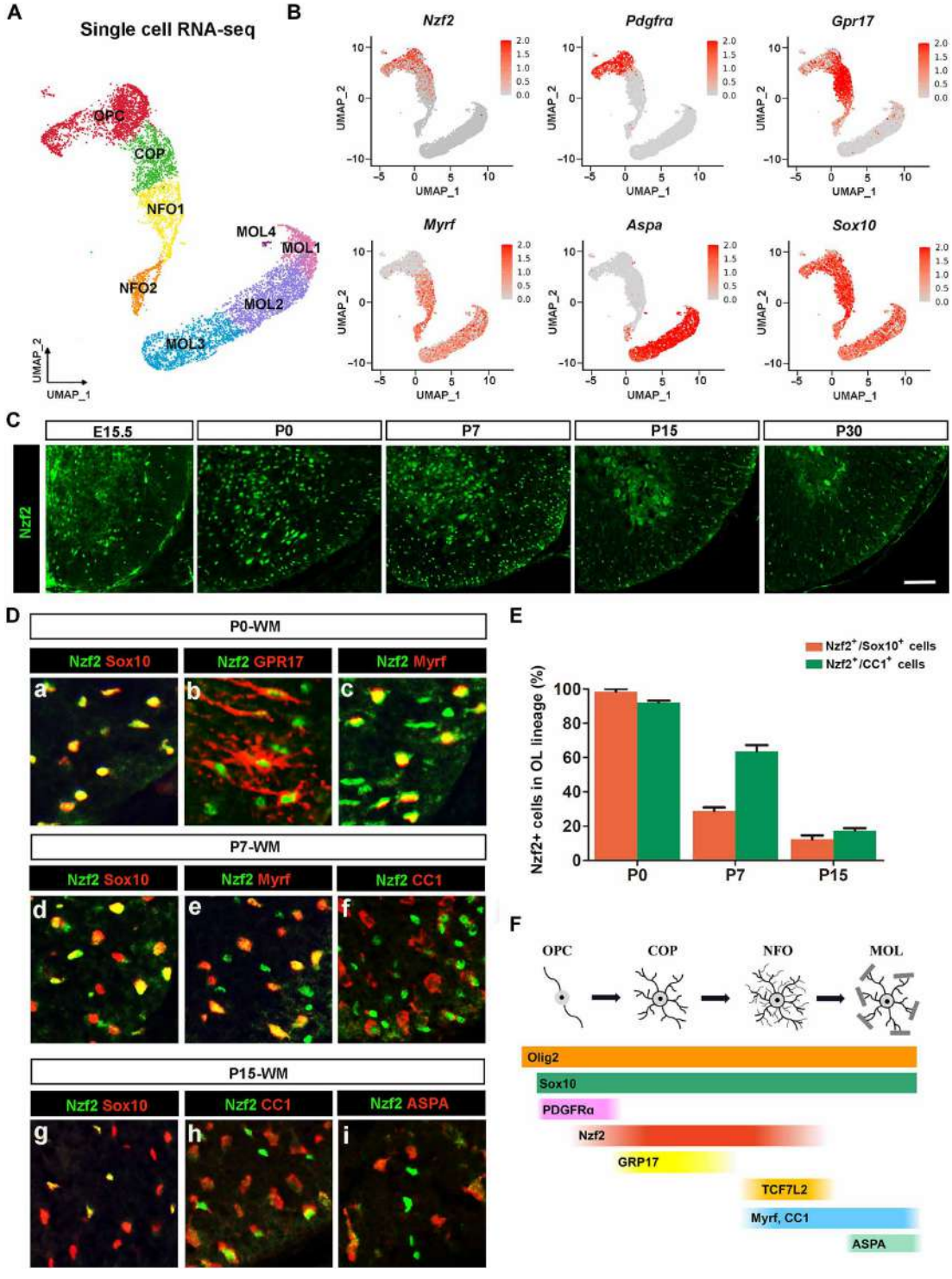

Fig. 1. Nzf2 is highly enriched in late OPCs and NFOs. (**A**) scRNA-seq of OL lineage cells isolated from spinal cords of wild-type mice at E15.5, P4, and P15. UMAP showing the trajectory from OPCs to MOLs. (**B**) Representative transcription levels of Nzf2 and other oligodendroglial markers on the UMAP map (gray, low expression; red, high expression). (**C**) Immunostaining of Nzf2 in the spinal cords of wild-type mice at E15.5, P0, P7, P15, and P30. (**D**) Double immunostaining of Nzf2 with different oligodendroglial markers (Sox10, GPR17, Myrf, CC1, and ASPA) in the spinal cords of wild-type mice at P0, P7, and P15. WM, white matter. (**E**) Quantification of the percentage of Nzf2/Sox10 double-positive cells (orange) or Nzf2/CC1 double-positive cells (green) among the total Sox10-positive or CC1-positive cells in the spinal cords of wild-type mice at P0, P7, and P15, respectively. (**F**) Diagram of OL development and stage-specific markers. Error bars indicate SEM. Scale bar, 100 μm.

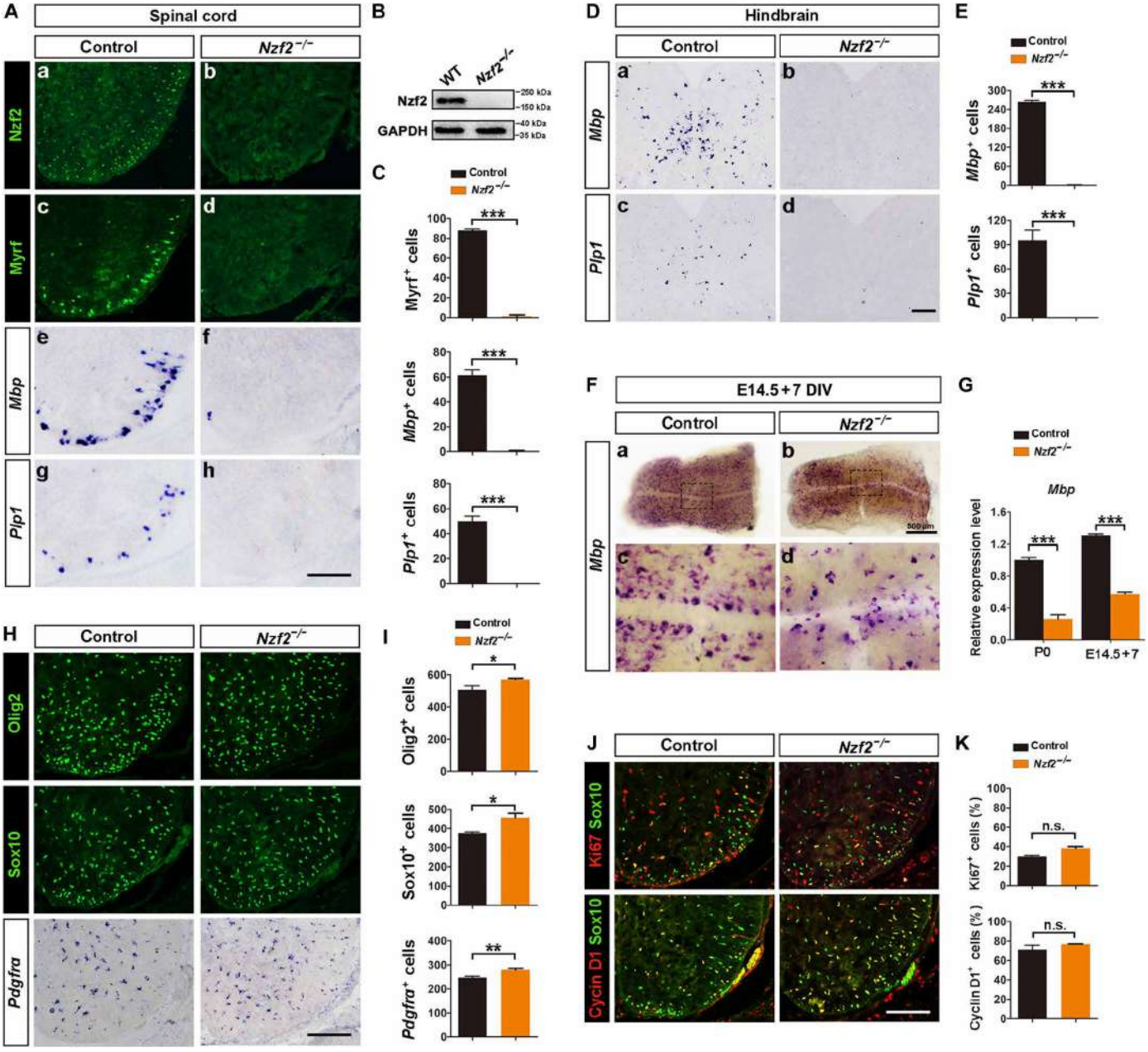

Fig. 2. *Nzf2* ablation leads to a marked delay in the initiation of OL differentiation. (**A**) Immunostaining of Nzf2, Myrf, and ISH of *Mbp* and *Plp1* in the spinal cords of control and $Nzf2^{-/-}$ mice at P0. (**B**) Western blot of Nzf2 expression in the brain of control and $Nzf2^{-/-}$ mice at P0. WT, wild type. (**C**) Quantification of $Myrf^+$, Mbp^+, and $Plp1^+$ cells per section in the spinal cords of control and $Nzf2^{-/-}$ mice at P0 from (A). (**D**) ISH of *Mbp* and *Plp1* in the hindbrain of control and $Nzf2^{-/-}$ mice at P0. (**E**) Quantification of Mbp^+ and $Plp1^+$ cells per section in the hindbrain of control and $Nzf2^{-/-}$ mice at P0 from (D). (**F**) Whole-mount ISH of *Mbp* in the spinal cord explants from control and $Nzf2^{-/-}$ mice at E14.5 and cultured in vitro for 7 days. Scale bar, 500 μm. DIV, days in vitro. (**G**) Quantification of *Mbp* expression levels in the spinal cord explant culture from control and $Nzf2^{-/-}$ mice. (**H**) Immunostaining of Olig2, Sox10, and ISH of *Pdgfrα* in the spinal cords of control and $Nzf2^{-/-}$ mice at P0. (**I**) Quantification of Olig2-positive, Sox10-positive, and *Pdgfrα*-positive cells per section in the spinal cords of control and $Nzf2^{-/-}$ mice at P0 from (H). (**J**) Double immunostaining of Ki67 and Sox10 and cyclin D1 and Sox10 in the spinal cords of control and $Nzf2^{-/-}$ mice at P0. (**K**) Quantification of the percentage of Ki67/Sox10 double-positive cells and cyclin D1/Sox10 double-positive cells among the total Sox10-positive cells in the spinal cords of control and $Nzf2^{-/-}$ mice at P0 from (J). Error bars indicate SEM. $*P \leq 0.05$, $**P \leq 0.005$, and $***P \leq 0.001$. n.s., no significant difference; GAPDH, glyceraldehyde phosphate dehydrogenase. Scale bars, 100 μm.

Flag-tagged Nzf2 protein were used to infect CG4 cells, and stable transfectants were selected using G418. The addition of Dox into the culture medium rapidly triggered the expression of Nzf2/Flag (Fig. 3A). Following G418 selection, immunostaining revealed that the purity of $Flag^+$ cells exceeded 96% (Fig. 3B). Western blot analysis confirmed the induced expression of Flag-tagged Nzf2 in CG4 cells (Fig. 3C). Nzf2 exhibited a basal level of endogenous expression in CG4 cells (fig. S3A). Upon Dox induction, a pronounced nuclear Nzf2 immunostaining signal was detected (fig. S3A). In the differentiation assay, T3 (triiodothyronine) was supplemented to the culture medium to augment differentiation. Expression of distinct OL marker genes was assessed at 3 or 5 days postdifferentiation (3 ddiff or 5 ddiff). Under these conditions, normal CG4 cells did not commence differentiation until 5 ddiff or beyond. Notably, Nzf2 hyperactivation led to precocious expression of myelin-associated glycoprotein (MAG) as early as 3 ddiff (Fig. 3D) and augmented MAG expression at 5 ddiff (Fig. 3F), as evidenced by the markedly elevated level of *Mag* expression (Fig. 3, E and G). Enhanced immunostaining of additional OL markers, myelin basic protein (MBP) and proteolipid protein 1 (PLP1), further corroborated the robust induction of OL differentiation by Nzf2 (fig. S3, B to D). Collectively, these findings indicated an accelerated transition of OPCs into OLs upon Nzf2 overexpression, implicating Nzf2 as a positive modulator of OL differentiation.

To validate the effect of Nzf2 on OL differentiation in vivo, we overexpressed the Nzf2 protein in the chicken spinal cord at embryonic day 2 (cE2) via in ovo electroporation (Fig. 3H). This overexpression also resulted in precocious *Mbp* and *Plp1* expression on the electroporated side at cE7 and cE9 (Fig. 3, I and J). Furthermore, the induced Mbp^+ or $Plp1^+$ cells in the ventral white matter colocalized with the Copepoda green fluorescent protein (CopGFP) or Flag signal (Fig. 3, I and J, arrowheads), suggesting that Nzf2 induces precocious OL differentiation in a cell-autonomous fashion.

Nzf2 promotes remyelination after demyelinating injury

The primary obstacle to axonal remyelination in demyelinating diseases lies in the limited capacity of adult OPCs to differentiate effectively into mature OLs (*31*). Our research findings reveal that the overexpression of Nzf2 stimulates OL differentiation, indicating a potential role for Nzf2 in promoting remyelination. To investigate this further, we induced focal demyelination in the corpus callosum of adult mouse brains by stereotactically injecting lysophosphatidylcholine (LPC) (Fig. 3K). Lentiviruses expressing Flag-tagged Nzf2 protein were administrated 3 days postlesion (dpl). We then analyzed the injury sites at various time points following lesion induction (Fig. 3K). TrueGold myelin staining demonstrated that, while the lesion sizes were comparable between control and Nzf2-overexpressed mice in the early stages postinjury (7 dpl), by 10 dpl, the lesion sizes were notably reduced in Nzf2-overexpressing mice compared to controls (Fig. 3, L and N). This suggests that Nzf2 accelerates the rate of remyelination. Consistent with this, we observed a significantly higher number of $Sox10^+$ and $CC1^+$ cells in the lesion sites of Nzf2-overexpressed mice compared to controls (Fig. 3, M and O). In addition, we also examined cell apoptosis after demyelinating injury, specifically within the OL lineage. Using terminal deoxynucleotidyl transferase–mediated deoxyuridine triphosphate nick end labeling (TUNEL) assays, we found that the majority of apoptotic cells at the lesion sites were $Iba1^+$ microglia (fig. S3E). Furthermore, no significant differences in cell apoptosis were observed following Nzf2 overexpression (fig. S3F). Overall, these findings imply that the overexpression of Nzf2 can substantially enhance OL differentiation and remyelination following demyelinating insults, offering a promising therapeutic approach for myelin repair.

Nzf2 mutation suppresses the expression of a core network of OL differentiation genes

On the basis of our observation that misexpression of Nzf2 altered the timing of OL differentiation, we sought to identify Nzf2-regulated downstream genes by conducting bulk RNA sequencing (RNA-seq) on P0 spinal cords from $Nzf2^{-/-}$ and wild-type mice. Our analysis revealed a total of 461 up-regulated and 644 down-regulated genes ($P \leq 0.05$) in *Nzf2*-deficient mice compared to wild-type littermates (fig. S4A; listed in table S1). Consistent with the differentiation defects observed in $Nzf2^{-/-}$ mice, the expression of myelin genes (*Mbp*, *Plp1*, and *Mag*) and OL differentiation–related genes (*Nkx2.2*, *Myrf*, *Enpp6*, and *Sirt2*) was significantly reduced in *Nzf2* mutants (Fig. 4A). Gene ontology (GO) analysis of the down-regulated genes indicated enrichment in glial cell differentiation and gliogenesis, aligning with the impaired OL differentiation in *Nzf2* KO mice (fig. S4B). Conversely, GO attributes linked to up-regulated genes focused on neuronal development (fig. S4C). The down-regulation of myelin-associated and differentiation regulators was further validated through real-time quantitative polymerase chain reaction (qRT-PCR; Fig. 4B). These RNA-seq data imply that Nzf2 directly or indirectly modulates a core network of genes crucial for OL differentiation.

To gain deeper insights into the direct targets of Nzf2, we carried our genome-wide mapping of Nzf2 binding sites using chromatin immunoprecipitation sequencing (ChIP-seq) in CG4 cells. This analysis identified 14,102 binding sites ($P \leq 0.01$) associated with 6204 unique genes, based on the nearest gene annotation (listed in table S2). The majority of Nzf2 binding sites were located within intronic regions, while a smaller but significant portion was found at gene promoter regions (Fig. 4C). In addition, we observed a pronounced enrichment of Nzf2 binding around transcription start sites (TSSs) (Fig. 4D), suggesting that Nzf2 primarily targets promoter/enhancer regions to regulate gene expression. By integrating these data with RNA-seq dataset, we pinpointed several genes that exhibited prominent Nzf2 binding within their genomic sequences and significant down-regulation of gene expression in $Nzf2^{-/-}$ mice (Fig. 4E; listed in table S3). GO analysis of these target genes confirmed their high enrichment in biological functions related to gliogenesis, OL development, and axon ensheathment (Fig. 4F). These genes include transcription factors controlling OL differentiation (e.g., *Nkx2.2* and *Sirt2*) (Fig. 4G). Together, these findings demonstrate that Nzf2 primarily functions as a transcriptional activator to facilitate OL differentiation.

Contrary to the previous in vitro findings (*25*), Nzf2 did not bind directly to the *Plp1* genomic sequence (Fig. 4H). Neither did it bind to the genomic sequences of another myelin gene *Mog* and the myelin regulatory factor *Myrf* (Fig. 4H) which activates the expression of myelin genes. These results imply that Nzf2 may not function to directly stimulate myelin gene expression as previously thought.

Nkx2.2 is a critical downstream target directly activated by Nzf2

Among the direct targets of Nzf2 identified, Nkx2.2 stands out as a prime candidate for regulating the timing of OL differentiation. This

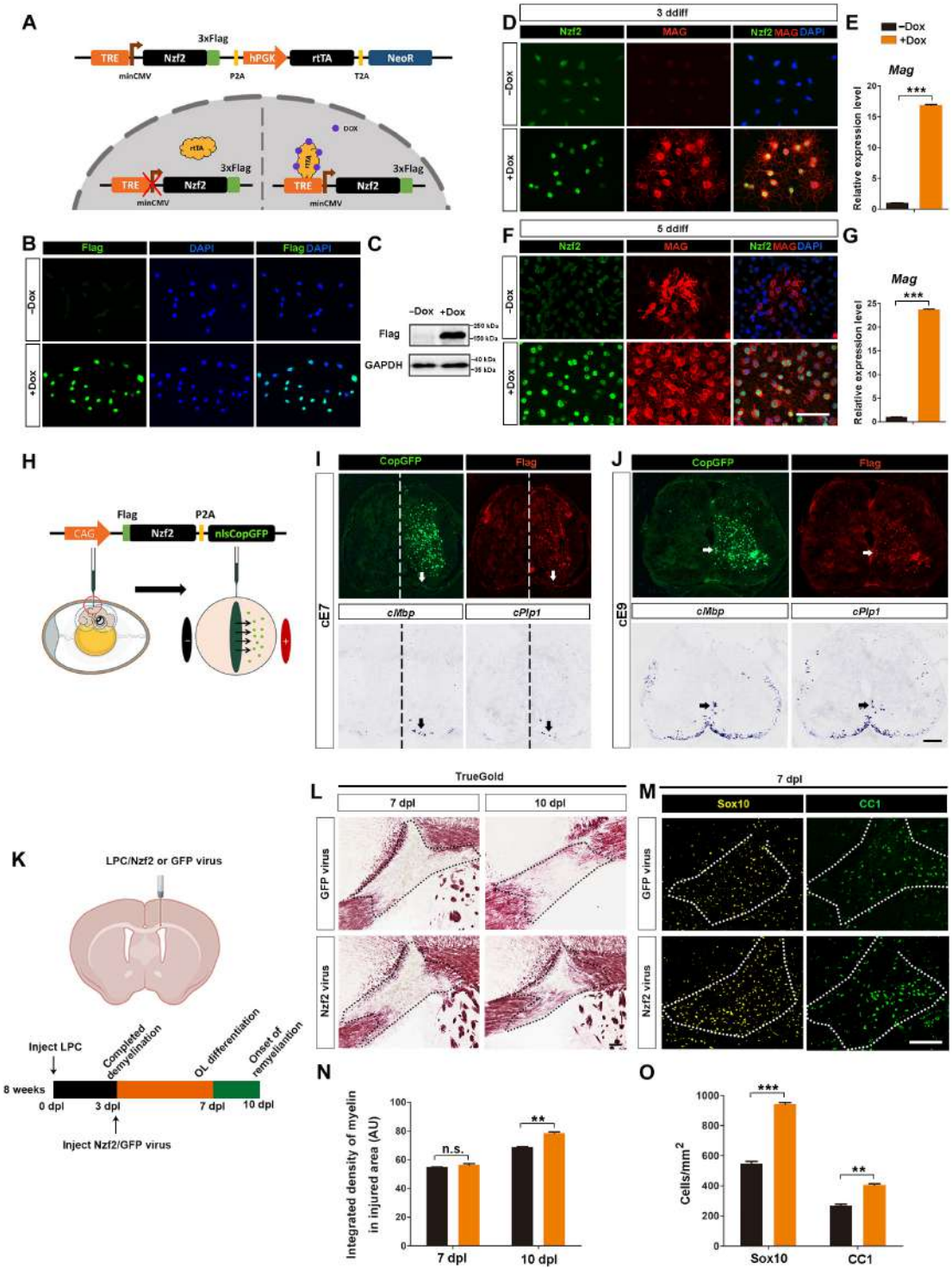

Fig. 3. Overexpression of Nzf2 induces precocious OL differentiation and promotes myelin repair. (**A**) Schematic diagram of the Dox-induced Nzf2 overexpression system. TRE, tetracycline response element; hPGK, human phosphoglycerate kinase promoter; NeoR, neomycin resistance; miniCMV, minimal cytomegalovirus promoter. (**B**) Immunostaining of Flag in CG4 cells in the proliferation medium with or without Dox treatment. Nuclei were stained with 4′,6-diamidino-2-phenylindole (DAPI). (**C**) Western blot of Flag in CG4 cells with or without Dox treatment. (**D**) Double immunostaining of Nzf2 (green) and MAG (red) in CG4 cells in the differentiation medium with or without Dox treatment at 3 ddiff. Nuclei were stained with DAPI. (**E**) Real-time quantitative polymerase chain reaction (qRT-PCR) analysis of *Mag* expression levels in CG4 cells with or without Dox treatment from (D). (**F**) Double immunostaining of Nzf2 (green) and MAG (red) in CG4 cells in the differentiation medium with or without Dox treatment at 5 ddiff. Nuclei were stained with DAPI. (**G**) qRT-PCR analysis of *Mag* expression levels in CG4 cells with or without Dox treatment from (F). (**H**) Schematic representation of in ovo electroporation of chicken embryos. (**I** and **J**) Immunostaining of Flag and ISH of *cMbp* and *cPlp1* in the spinal cords of chicken embryos at cE7 and cE9. The electroporated side is at right. Arrowheads points to the ectopic induced OLs. (**K**) Schematic representation of the lysophosphatidylcholine (LPC)–induced focal demyelination model and virus administration. (**L**) TrueGold myelin staining of GFP virus– and Nzf2 virus–injected injury areas at 7 dpl and 10 dpl. (**M**) Immunostaining of Sox10 and CC1 in GFP virus– and Nzf2 virus–injected injury areas at 7 dpl. (**N**) Quantification of the myelin density in injury areas (square micrometers) from (L). (**O**) Quantification of $Sox10^+$ and $CC1^+$ cell density (calculated per square millimeter) at 7 dpl from (M). Error bars indicate SEM. $^{**}P \leq 0.005$ and $^{***}P \leq 0.001$. Scale bar: 100 μm. AU, arbitrary units.

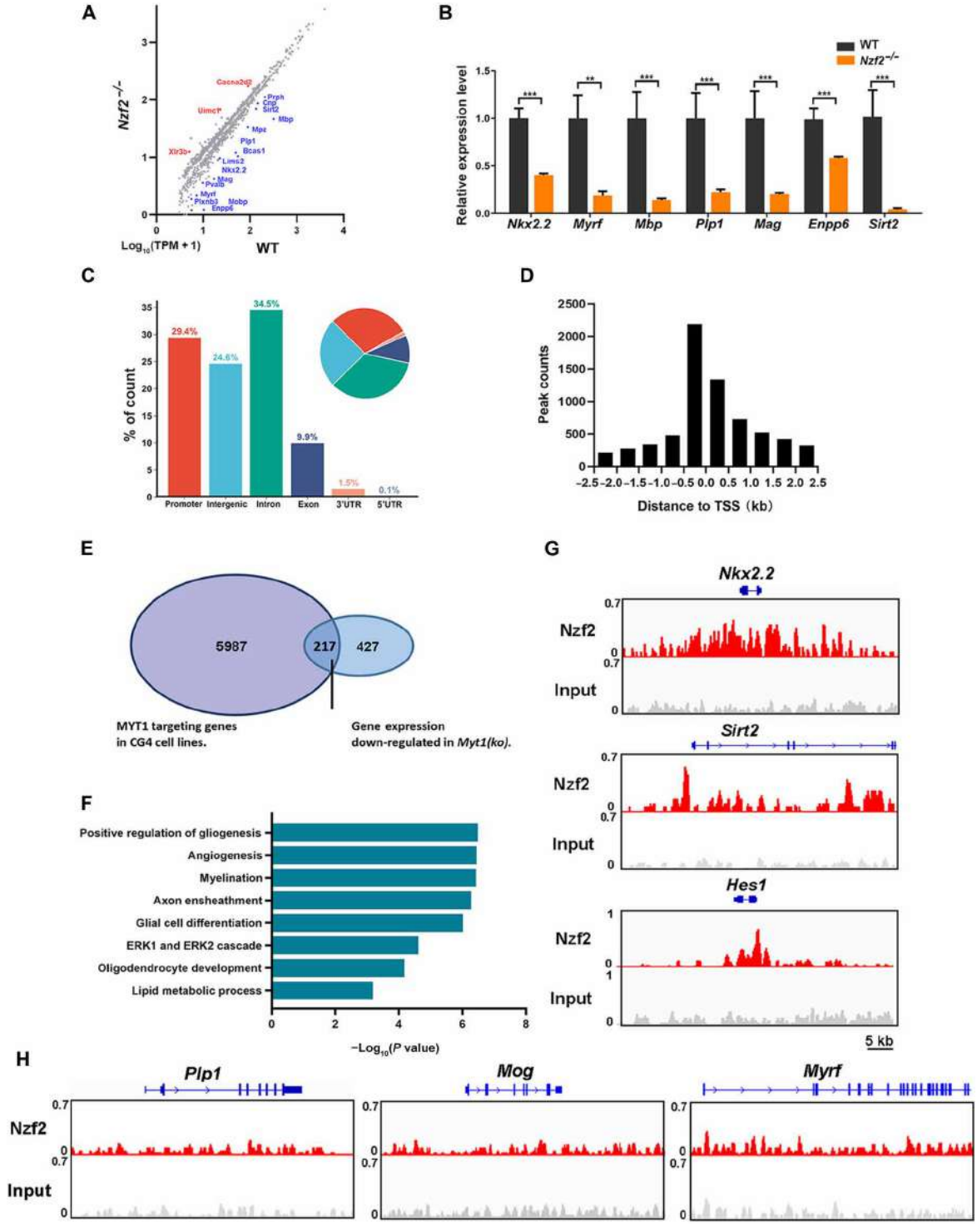

Fig. 4. Nzf2 regulates a core network of genes that drive OL differentiation. (**A**) Volcano plots depict gene expression changes between wild-type (WT) and *Nzf2*$^{-/-}$ spinal cords at P0. Significantly differential transcripts were highlighted in color and totaled in each direction. TPM, transcripts per million reads. (**B**) qRT-PCR validation of oligodendroglial-associated genes in the spinal cords of WT and *Nzf2*$^{-/-}$ mice at P0. (**C**) Fraction of Nzf2 ChIP-seq peaks in different regions of genome. (**D**) Histogram showing the distribution of ChIP-seq peaks relative to the transcription start sites (TSSs). (**E**) Venn diagram showing the overlap between Nzf2-bound genes and down-regulated genes in the spinal cords of *Nzf2*$^{-/-}$ mice at P0. (**F**) GO analysis of Nzf2 directly activated genes. (**G**) The enrichment of Nzf2 at selected gene loci (*Nkx2.2*, *Sirt2*, and *Hes1*). (**H**) Nzf2 ChIP-seq analysis at promoter regions of myelin-related genes (*Plp1*, *Mog*, and *Myrf*). Error bars indicate SEM. $^{**}P \leq 0.005$ and $^{***}P \leq 0.001$. 3′UTR, 3′ untranslated region; ERK1, extracellular signal–regulated kinase.

is supported by the fact that the reported phenotypes of *Nkx2.2* loss- and gain-of-function models closely mirror those of *Nzf2* (*21*, *22*). In support of this notion, Nzf2 expression precedes Nkx2.2 expression in the spinal cord during the stage of OL differentiation. At E15.5, a significant number of $Nzf2^+$ cells and a smaller number of $Nkx2.2^+$ cells started to emerge in the ventrolateral white matter (Fig. 5A, a and b), with some OPCs coexpressing both (Fig. 5A, c). This coexpression persisted in the white matter until birth (Fig. 5A, d to f). In $Nzf2^{-/-}$ spinal cords, Nkx2.2 expression in the white matter was completely abolished, while its expression in V3 interneurons remained normal (Fig. 5B). By contrast, Nzf2 expression was not significantly altered in the spinal cords of *Nkx2.2* cKO mice (Fig. 5, C and D). These results strongly suggest that Nzf2 acts upstream of Nkx2.2 to regulate OL differentiation. Furthermore, overexpression of Nzf2 in CG4 cells significantly increased Nkx2.2 expression levels (Fig. 5E). These functional analyses demonstrated that Nzf2 is both necessary and sufficient for activating Nkx2.2 expression.

To further investigate the regulatory relationship between Nzf2 and Nkx2.2, we conducted ChIP-qPCR analyses and confirmed multiple bindings of Nzf2 at the *Nkx2.2* proximal promoter region (Fig. 5, F and G). A de novo search of Nzf2 ChIP-seq data identified enrichment of the AAG/CTT motif at peak summits (Fig. 5H). To test the direct binding of Nzf2 to *Nkx2.2* promoter regions, we performed an electrophoretic mobility shift assay (EMSA) using a *Nkx2.2* oligonucleotide probe spanning the AAG/CTT motif or a mutated version (Fig. 5I). Our results showed that Nzf2 directly binds to the *Nkx2.2* promoter sequence through the AAG/CTT motif (Fig. 5J).

To further validate the hypothesis that Nkx2.2 functions downstream of Nzf2 in regulating OL differentiation, we generated the *PDGFRα-creERT2*; *R26-Nkx2.2* mice (referred to *Nkx2.2* overexpression, *Nkx2.2* OE) (Fig. 5K). When tamoxifen was administrated to pregnant *Nkx2.2* OE mice from E15.5 to E17.5 (Fig. 5L), robust Nkx2.2 expression was induced in OPCs as expected [Fig. 5, M (c) and N]. Concurrently, supernumerary MBP^+ cells were observed in the white matter of Nkx2.2 OE embryos compared to the control tissues [Fig. 5, M (d) and O]. Contrary to the complete loss of Mbp^+ cells in $Nzf2^{-/-}$ embryos (Fig. 2A, f), a small number of MBP^+ OLs emerged in the white matter of $Nzf2^{-/-}$; *Nkx2.2* OE embryos [Fig. 5, M (f) and O]. This result strongly indicated that induced expression of Nkx2.2 in platelet-derived growth factor receptor-α $(PDGFRα)^+$ OPCs is able to, at least partially, rescue the differentiation defect of OPCs in $Nzf2^{-/-}$ mice.

Nzf2 epigenetically promotes OL differentiation through antagonizing histone deacetylation

Previous studies have indicated that numerous zinc finger–containing transcription factors epigenetically regulate downstream gene expression (*32*–*35*). Given the pivotal role of histone modification in initiating OL differentiation (*36*, *37*), we subsequently investigated the impact of Nzf2 expression on the histone acetylation of H3K9 and H3K27, two critical histone modification events for the transcriptional regulation of OL development (*38*–*40*). Through comparative ChIP-seq analyses of H3K9ac, H3K27ac, and Nzf2, we discovered that Nzf2 binds to a substantial proportion of H3K9ac (54.8%, 1260 of 2300) and H3K27ac (59%, 1912 of 3239) sites within many OL-related genes, including *Nkx2.2* and *Sirt2* (Fig. 6A). Notably, a pronounced enrichment of Nzf2 binding was observed around TSSs within ~2-kb promoter regions of these genes (Fig. 6B), and Nzf2 motifs were highly enriched at H3K9ac and H3K27ac modification sites (Fig. 6, C and D). These findings strongly implicate Nzf2 in regulating downstream gene expression by enhancing histone acetylation.

To further explore this possibility, we compared H3K9ac and H3K27ac levels in control and Nzf2 OE cells. As anticipated, ChIP-qPCR analysis revealed substantial higher acetylation levels of histones, particularly H3K9, at Nzf2-bound *Nkx2.2* promoter regions upon Nzf2 overexpression (Fig. 6E). As a negative control, the promoter region of *Hes1*, which was strongly bound by Nzf2 (Fig. 4G) (*29*), exhibited no H3K9ac or H3K27ac modifications (fig. S5A). Furthermore, there was no significant difference in *Hes1* expression between wild-type and $Nzf2^{-/-}$ mice (fig. S5B). These results strongly suggest that Nzf2 elevates histone acetylation at its binding loci, thereby enhancing the transcription of OL differentiation–related genes. Consistent with this notion, treatment of CG4 cells with trichostatin A (TSA), an HDAC inhibitor (fig. S5, C and D) (*41*), increased *Nkx2.2* expression and prompted OL differentiation (fig. S5, E and F), reminiscent of the findings observed in Nzf2 overexpression studies (Figs. 3, D and F, and 5E). Moreover, TSA-treated cells exhibited a more mature OL morphology compared to untreated cells (fig. S5E, d). Thus, Nkx2.2 expression is under the regulation of histone acetylation, and derepression of histone acetylation is able to induce OL differentiation and maturation.

Subsequently, we explored the mechanism underlying Nzf2's binding on local histone acetylation. Given that histone acetylation is determined by the balance between histone acetyltransferases (HATs) and HDACs (fig. S5C), we examined the potential protein interactions between Nzf2 and these enzymes. In human embryonic kidney (HEK) 293T cells transfected with Nzf2-3×Flag, we observed that Flag-conjugated beads were able to pull down cotransfected HDAC1 (Fig. 6F) but not general control non-derepressible 5 protein (GCN5) (Fig. 6G), a HAT complex member known to specifically acetylate H3K9 (*42*). To further validate this interaction, we also conducted endogenous Nzf2 immunoprecipitation (IP) using protein A/G beads and confirmed that Nzf2 interacts with endogenous HDAC1 but not GCN5 (Fig. 6H). Co-IP analyses with other HDAC family members demonstrated that Nzf2 exhibits a strong and specific physical interaction with HDAC1 but only weak interactions with HDAC2 or HDAC3 (fig. S5, G and H). It is well-established that HDAC1 is a major component of three distinct repressor complexes [Sin3, nucleosome remodeling and deacetylation complex (NuRD), and CoREST] (Fig. 6I) (*43*). Notably, we found that the interaction of Nzf2 with HDAC1 markedly attenuated HDAC1 binding to Sin3A, retinoblastoma binding protein 4 (RBBP4), and CoREST and consequently blocked the assembly of these repressor complexes in a dose-dependent manner (Fig. 6J). Therefore, Nzf2 inhibits the assembly of HDAC1 repressor complexes via competitive binding.

Given the detected strong interaction between Nzf2 and HDAC1, we analyzed the structural basis of Nzf2-HDAC1 interaction through the protein-protein docking platform (https://hermite.dp.tech, Hermite Platform, DP Technology). According to the reported electron microscopy structure information of NuRD complex (*44*), the active sites or the deacetylase center of HDAC1 are exposed to exterior space (Fig. 6K). When physically interacting with Nzf2, HDAC1 adopts a compact state with the active sites buried inside and functionally blocked (Fig. 6K). Consistently, the deacetylation activity of HDAC1 was reduced in the presence of purified Nzf2 protein (Fig. 6L). Thus, Nzf2 binding altered the HDAC1 protein structure and restricted

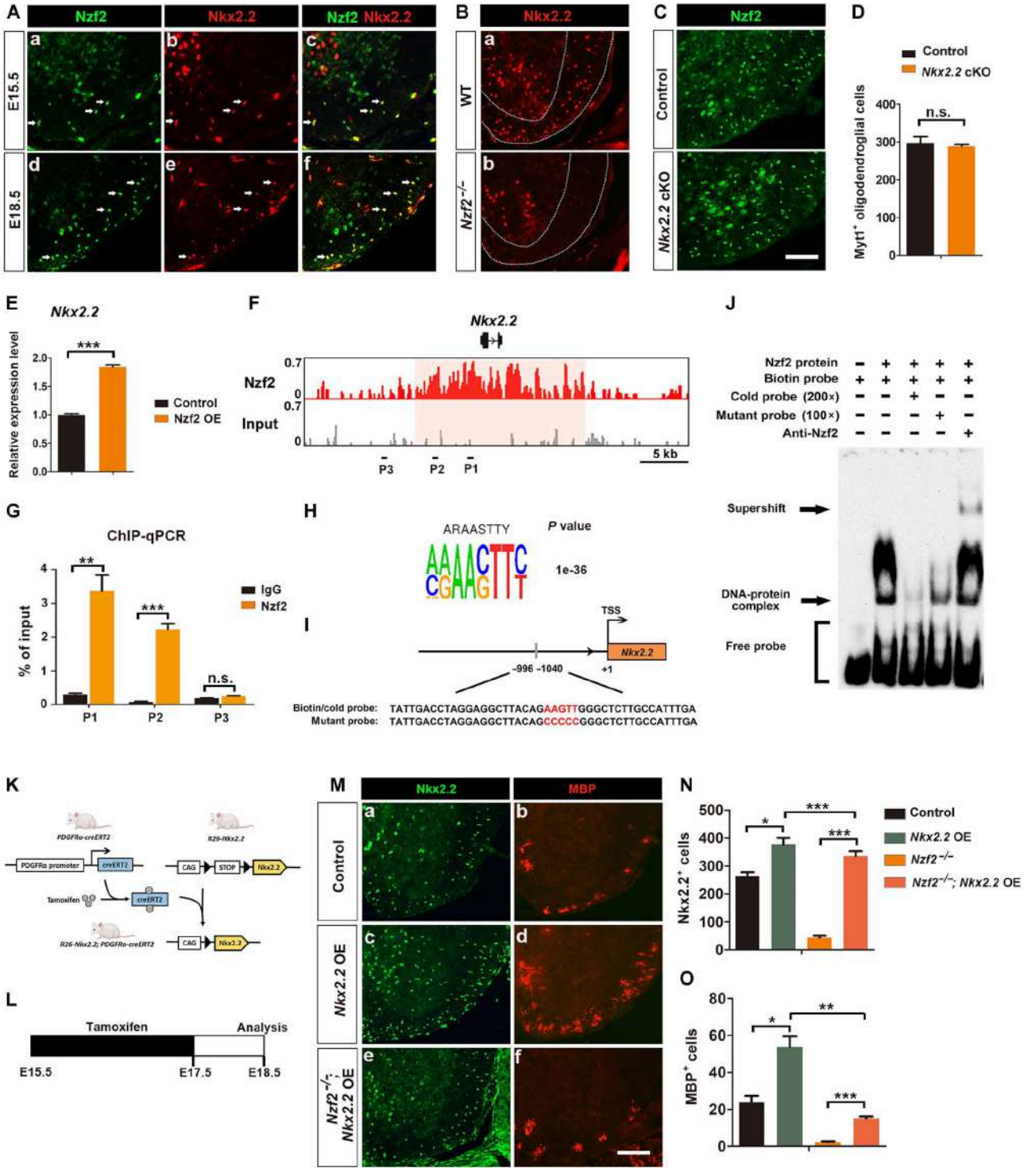

Fig. 5. *Nkx2.2* is a downstream effector gene directly activated by Nzf2. (**A**) Double immunostaining of Nzf2 (green) and Nkx2.2 (red) in the spinal cords of wild-type embryos at E15.5 and E18.5. (**B**) Immunostaining of Nkx2.2 in the spinal cords of wild-type and *Nzf2*$^{-/-}$ mice at P0. The white matter area was outlined by dashed lines. (**C**) Immunostaining of Nzf2 in the spinal cords of the control (*Nkx2.2*$^{fx/+}$; *Olig1*^{cre}) and *Nkx2.2* cKO (*Nkx2.2*$^{fx/fx}$; *Olig1*^{cre}) animals at E18.5. (**D**) Quantification of Nzf2/Sox10 double-positive cells per section in the spinal cords of control and *Nkx2.2* cKO mice at E18.5 from (C). (**E**) qRT-PCR analysis of *Nkx2.2* expression levels in CG4 cells with or without Nzf2 overexpression. (**F**) The enrichment of Nzf2 at *Nkx2.2* gene loci. (**G**) ChIP-qPCR analysis of the enrichment of distinct regions (P1, P2, and P3) distributed throughout the *Nkx2.2* gene locus in input and precipitated chromatin with immunoglobulin G (IgG) or anti-Nzf2 antibody. (**H**) Top overrepresented Nzf2 binding motif AA[G/C]TT. (**I**) Schematic diagram of the genomic sequence upstream of *Nkx2.2* for the EMSA probe. The core site AAGTT (red) was replaced with CCCCC as the mutant probe. (**J**) EMSA analysis of Nzf2 binding. The bottom arrow shows the Nzf2-probe complexes with lower mobility. The top arrow marks Nzf2–probe–Nzf2 antibody complexes with the lowest mobility. (**K**) Schematic diagram of generation of *PDGFRα-creERT2; R26-Nkx2.2* mice to induce Nkx2.2 overexpression in OPCs by tamoxifen injection. (**L**) Time windows of tamoxifen treatment. (**M**) Immunostaining of Nkx2.2 and MBP in the spinal cords of control, *Nkx2.2* OE (*PDGFRα-creERT2; R26-Nkx2.2*), and *Nzf2*$^{-/-}$; *Nkx2.2* OE mice at E18.5. (**N** and **O**) Quantification of Nkx2.2- and MBP-positive cells per section in the spinal cords of control, *Nkx2.2* OE, *Nzf2*$^{-/-}$, and *Nzf2*$^{-/-}$; *Nkx2.2* OE mice at E18.5. Error bars indicated SEM. *$P \leq 0.05$, **$P \leq 0.005$, and ***$P \leq 0.001$. Scale bars, 100 μm.

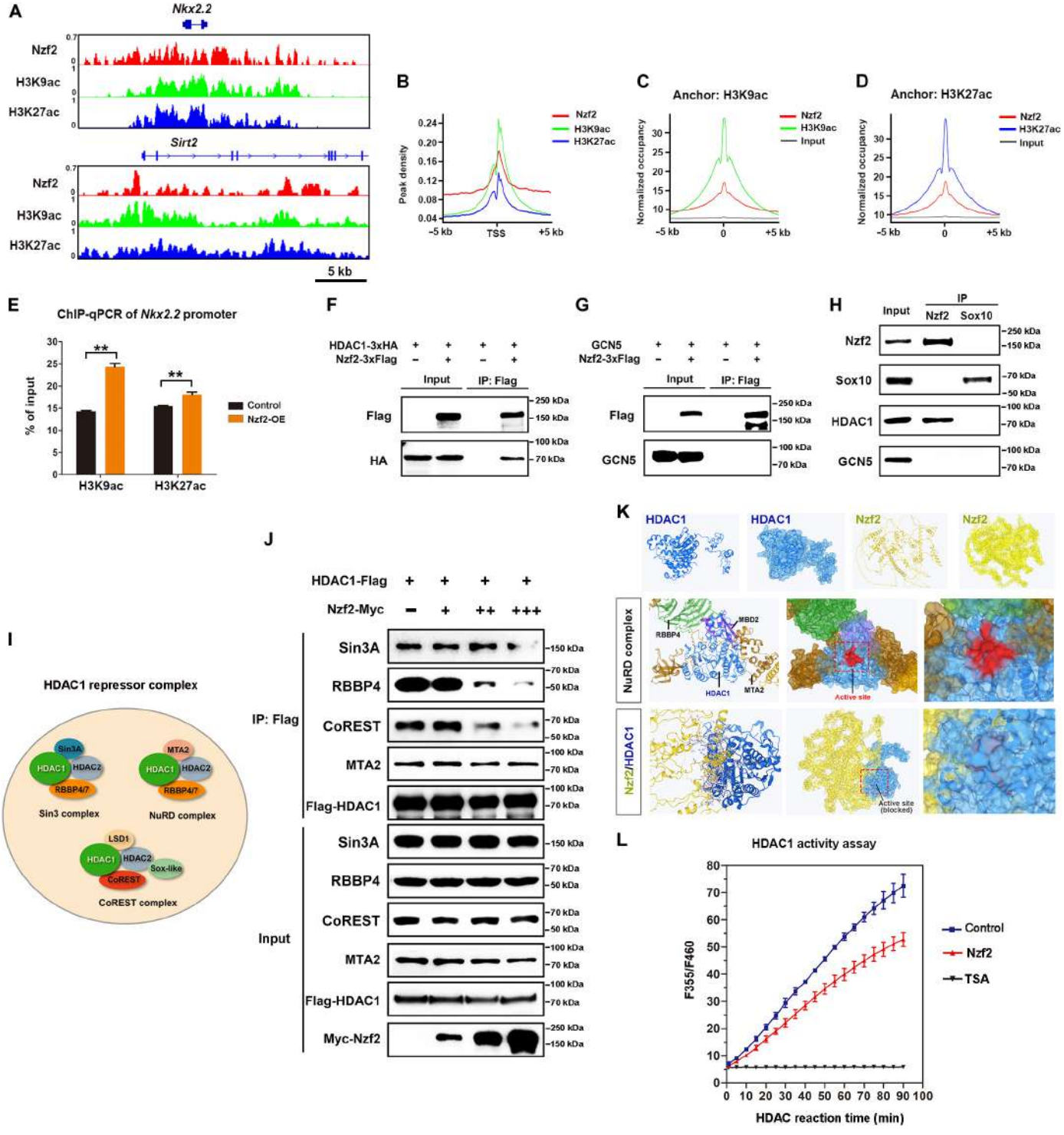

Fig. 6. Nzf2 epigenetically promotes OL differentiation through antagonizing histone deacetylation. (**A**) The enrichment of Nzf2 at the H3K9ac- and H3K27ac-modified gene loci (*Nkx2.2* and *Sirt2*). (**B**) The distribution of Nzf2-binding peaks, H3K9ac- and H3K27ac-modified peaks relative to TSS. (**C** and **D**) ChIP-seq binding profiles of Nzf2 around H3K9ac and H3K27ac peak summits. (**E**) H3K9ac and H3K27ac ChIP-qPCR analysis of *Nkx2.2* gene loci in control and Nzf2 OE CG4 cells. (**F**) Co-IP analysis of HDAC1-3×HA with Nzf2-3×Flag from transiently transfected HEK293T cells. (**G**) Co-IP analysis of GCN5 with Nzf2-3×Flag from transiently transfected HEK293T cells. (**H**) Endogenous Nzf2 and Sox10 IP analysis of HDAC1 and GCN5 with protein A/G beads. (**I**) Schematic diagram of the HDAC1 repressor complexes. (**J**) IP analysis of endogenous HDAC1 complex components (Sin3A, RBBP4, CoREST, and MTA2) with HDAC1-Flag from transiently Nzf2-myc–transfected HEK293T cells. (**K**) Three-dimensional structure of NuRD-HDAC1 complex and Nzf2-HDAC1 complex through protein-protein docking analysis. (**L**) HDAC1 activity analysis after adding control proteins (GFAP), Nzf2 proteins, or TSA. Errors bars indicated SEM. $^{**}P \leq 0.005$.

its deacetylase activity. These observations led us to propose that Nzf2 activates OL differentiation by suppressing HDAC1-mediated histone deacetylation. In line with this idea, HDAC1 overexpression in CG4 cells substantially attenuated the Nzf2-induced OL differentiation programs (fig. S5, I to K).

Nzf2 establishes an accessible chromatin landscape to promote downstream gene transcription

Since HDAC complexes modulate chromatin accessibility and gene expression through histone deacetylation, we speculate that Nzf2 acts to inhibit HDAC1-mediated deacetylation, thereby creating an accessible chromatin landscape for nearby gene expression. To comprehensively assess the global changes in chromatin accessibility upon *Nzf2* deletion, we collected spinal tissues from neonatal wild-type and *Nzf2*$^{-/-}$ mice and performed the transposase-accessible chromatin assay with high-throughput sequencing (ATAC-seq). By comparing the peak intensities at each locus between wild-type and *Nzf2*$^{-/-}$ mice, we observed that deletion of *Nzf2* led to altered chromatin accessibility in 8143 genes as expected (listed in table S4). Notably, more than 97% of them (7928 of 8143) exhibited decreased chromatin accessibility. Among the genes with diminished chromatin accessibility in *Nzf2*$^{-/-}$ spinal cords, more than 39% (3101 of 7928) were found to be Nzf2-bound, indicating the necessity of Nzf2 for chromatin remodeling. Deletion of *Nzf2* resulted in pronounced reduction in chromatin accessibility of the identified target genes (e.g., *Nkx2.2*) (fig. S6A). Overall, chromatin accessibility around TSS was markedly decreased in *Nzf2* mutant mice (fig. S6B). These findings collectively demonstrated that Nzf2 is essential for the establishing an accessible chromatin landscape of target genes, thereby facilitating the transcriptional progression of OLs.

Myt domain is responsible for HDAC1 interaction and dispensable for OL differentiation

The Nzf2 protein comprises two clusters of zinc finger domains, which are separated by a Myt domain (Fig. 7A). To delineate the structural domains of Nzf2 protein that mediate its role in OL differentiation, we constructed a series of systematic Nzf2 truncations (Fig. 7A). Our findings revealed that overexpression of truncated Nzf2 protein containing only one cluster of zinc finger domains, Nzf2 (556-1169) or Nzf2 (1-843), was capable of inducing precocious OL differentiation (Fig. 7B, d and f) but with substantially reduced efficiency compared to the full-length Nzf2 (Fig. 7C). These observations suggest that Nzf2 may interact with multiple DNA sites and that the zinc finger domains cooperate to facilitate DNA binding. Notably, deletion of the Myt domain (Nzf2 1-603) completely abolished its capacity to induce OL differentiation (Fig. 7B, h) and its interaction with HDAC1 (Fig. 7D). This indicates that the conserved Myt domain is indispensable for the physical interaction with HDAC1. Together, these results demonstrated that Nzf2 promotes OL differentiation through direct binding of the genomic AAG/CTT motif via its zinc finger domains and through physical interaction with HDAC1 by its central Myt domain.

Nzf2 functions downstream of Notch signaling to initiate OL differentiation

To further elucidate the upstream regulation of Nzf2 in controlling OPC differentiation and myelin development, we considered previous reports indicating that Notch signaling inhibits OL differentiation and myelin gene expression during early developmental stages (*23*, *24*, *45*). On the basis of this, we postulated that Nzf2 might promote OL differentiation by counteracting Notch signaling. Given that Notch1 and Hes5 are the major receptor and the downstream effector of the Notch signaling pathway in OPCs (*46*), we initially assessed their expression in *Nzf2*$^{-/-}$ mice and found no significant change between the control and mutant spinal tissues (fig. S7, A and B). This result hinted that Nzf2 functions downstream of the Notch pathway. To validate this hypothesis, we examined Nzf2 expression in *Sox10-rtTA*; *TetO-dnMaml1* double transgenic mice (hereinafter referred to as *dnMaml1* OE mice). In these mice, the dominant-negative form of Maml1 (dnMaml1), fused with enhanced green fluorescent protein (eGFP) at its C terminus, can be induced by Dox treatment in OL lineage cells. The dnMaml1 protein disrupts the transactivation activity of all Notch receptors by binding to the Notch-CSL (CBF1/Su[H]/Lag2 protein) transcriptional complex, thereby blocking its transcriptional activation of all target genes in OL lineage cells (Fig. 8A) (*47*, *48*). Specifically, Dox was administrated from E12.5 for 6 days, and spinal tissues were harvested at E18.5 for analysis of myelin gene expression (Fig. 8B). We observed efficient induction of eGFP signal upon Dox treatment (Fig. 8C, f and k). As reported previously (*24*), dnMaml1 overexpression resulted in pronounced precocious OL differentiation, with numerous premature *Mbp*$^{+}$ and *Plp1*$^{+}$ OLs appearing in the gray matter of transgenic spinal tissue (Fig. 8C, g and h). Ectopic Nzf2 expression was also induced in *dnMaml1* OE mice, particularly in the gray matter (Fig. 8C,i), and the number of Nzf2^{+} cells nearly doubled in the transgenic mice (Fig. 8D). As expected, the number of Nkx2.2^{+} cells also significantly increased in the gray matter of *dnMaml1* OE spinal cords (Fig. 8C, j). To further substantiate the idea that Nzf2 functions downstream of Notch signaling in regulating OL differentiation, we generated the double transgenic mice with a *Nzf2*$^{-/-}$ genetic background through sequential interbreeding. We found that deletion of Nzf2 in *dnMaml1* OE mice completely abrogated the formation of *Mbp*$^{+}$ and *Plp1*$^{+}$ OLs (Fig. 8C, l and m), confirming that Nzf2 is a pivotal downstream effector of Notch signaling in modulating OL differentiation.

In addition, we also expressed the constitutive-active form of Notch 1 (NICD) in CG4 cells, both in the absence and presence of Nzf2 coexpression (Fig. 8E). Quantitative analysis revealed a modest yet significantly down-regulation of *Nzf2* mRNA levels in NICD OE cells (Fig. 8G), further confirming that the Notch signaling pathway acts upstream of Nzf2 during OPC differentiation. In differentiation medium, untransfected CG4 cells started to differentiate at 6 ddiff and expressed MAG (Fig. 8F, c). NICD overexpression substantially inhibited spontaneous cell differentiation (Fig. 8F, f) and reduced the expression of *Mag* (Fig. 8H). However, concurrent overexpression of Nzf2 alleviated the inhibitory effects of NICD on cell differentiation (Fig. 8F, i) and *Mag* expression (Fig. 8H). Collectively, these results suggested that Nzf2 functions downstream of Notch signaling in regulating OL differentiation and myelin development.

DISCUSSION

The Nzf2/Myt1 zinc finger protein was initially recognized for its ability to bind to the promoter of human myelin proteolipid protein (*PLP*) gene and stimulate reporter gene expression in vitro (*25*). However, our current study uncovers that the Nzf2's principal role is to modulate the onset of OL differentiation, rather than directly enhancing myelin gene expression in MOLs. Nzf2 exerts no influence

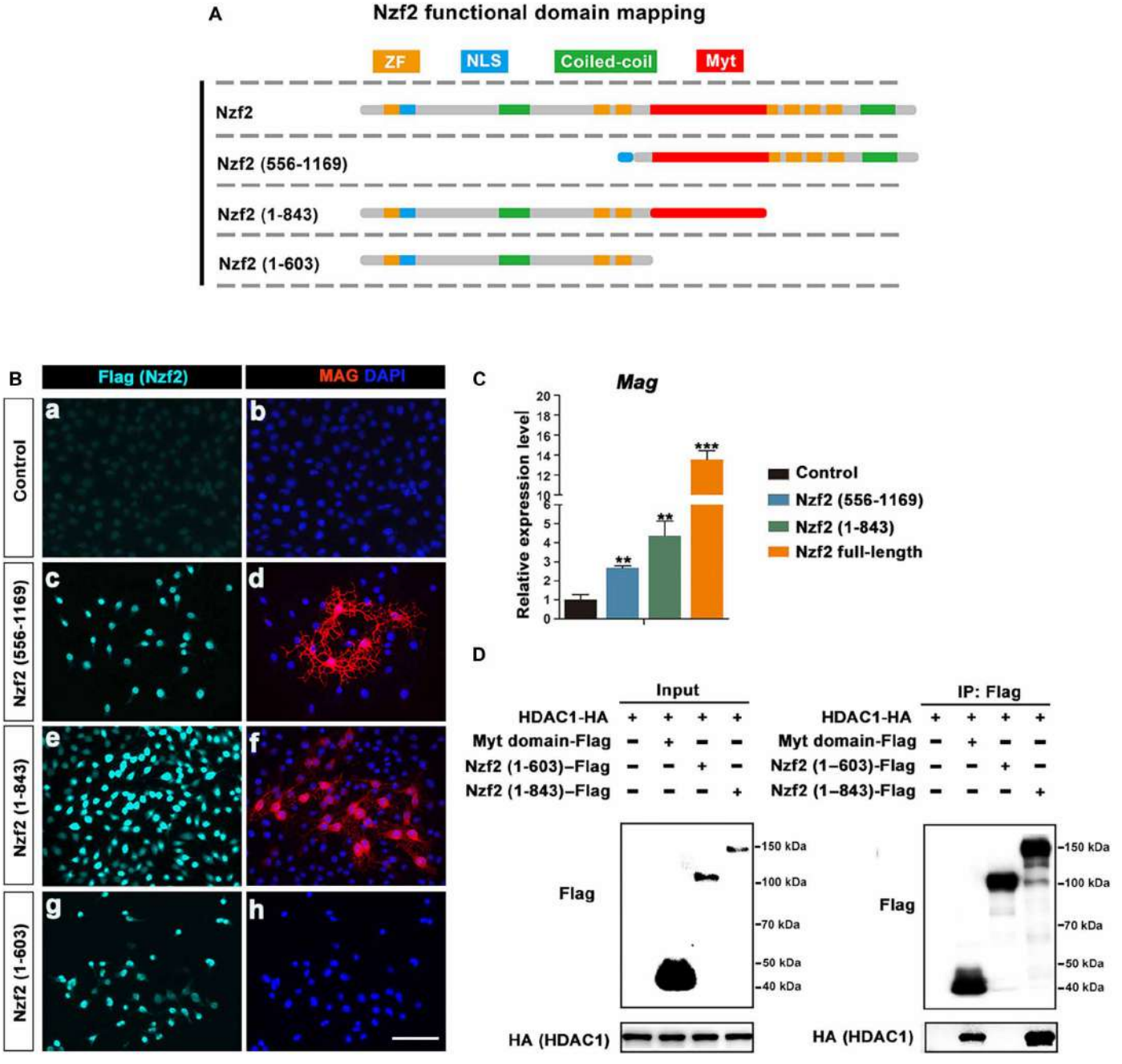

Fig. 7. Myt domain is responsible for HDAC1 interaction and dispensable for OL differentiation. (**A**) Schematic diagram of Nzf2 functional domains and different Nzf2 truncations. (**B**) Double immunostaining of Flag (blue) and MAG (red) in control, Nzf2 (556-1169)–, Nzf2 (1-843)–, and Nzf2 (1-603)–overexpressed CG4 cells at 5 ddiff. (**C**) qRT-PCR analysis of *Mag* expression levels in control, Nzf2(556-1169), Nzf2(1-843), and full-length Nzf2-overexpressed CG4 cells at 5 ddiff. (**D**) Co-IP analysis of HDAC1-HA with Myt domain-Flag, Nzf2 (1-603)–Flag, and Nzf2 (1-843)–Flag from transiently transfected HEK293T cells. Errors bars indicated SEM. $^{**}P \leq 0.005$ and $^{***}P \leq 0.001$. Scale bar, 100 μm.

on OPC proliferation and migration but instead directly promotes their differentiation. Consistent with this notion, Nzf2 expression is transiently up-regulated in late OPCs and postmitotic COPs yet promptly down-regulated in NFOs. Ablation of *Nzf2* leads to a profound delay in OL differentiation without affecting OPC specification or proliferation. Conversely, hyperactivation of Nzf2 induces precocious OL differentiation in the oligodendroglial cell line and embryonic spinal cords. Nzf2 overexpression facilitates remyelination following myelin injury.

Mechanistically, we present compelling genetic and molecular evidence that Nzf2 activates OL differentiation by stimulating the transcription of *Nkx2.2*, a crucial prodifferentiation factor, through the repression of HDAC1-mediated gene-specific histone deacetylation. In this study, we have delineated the intricate molecular cascade

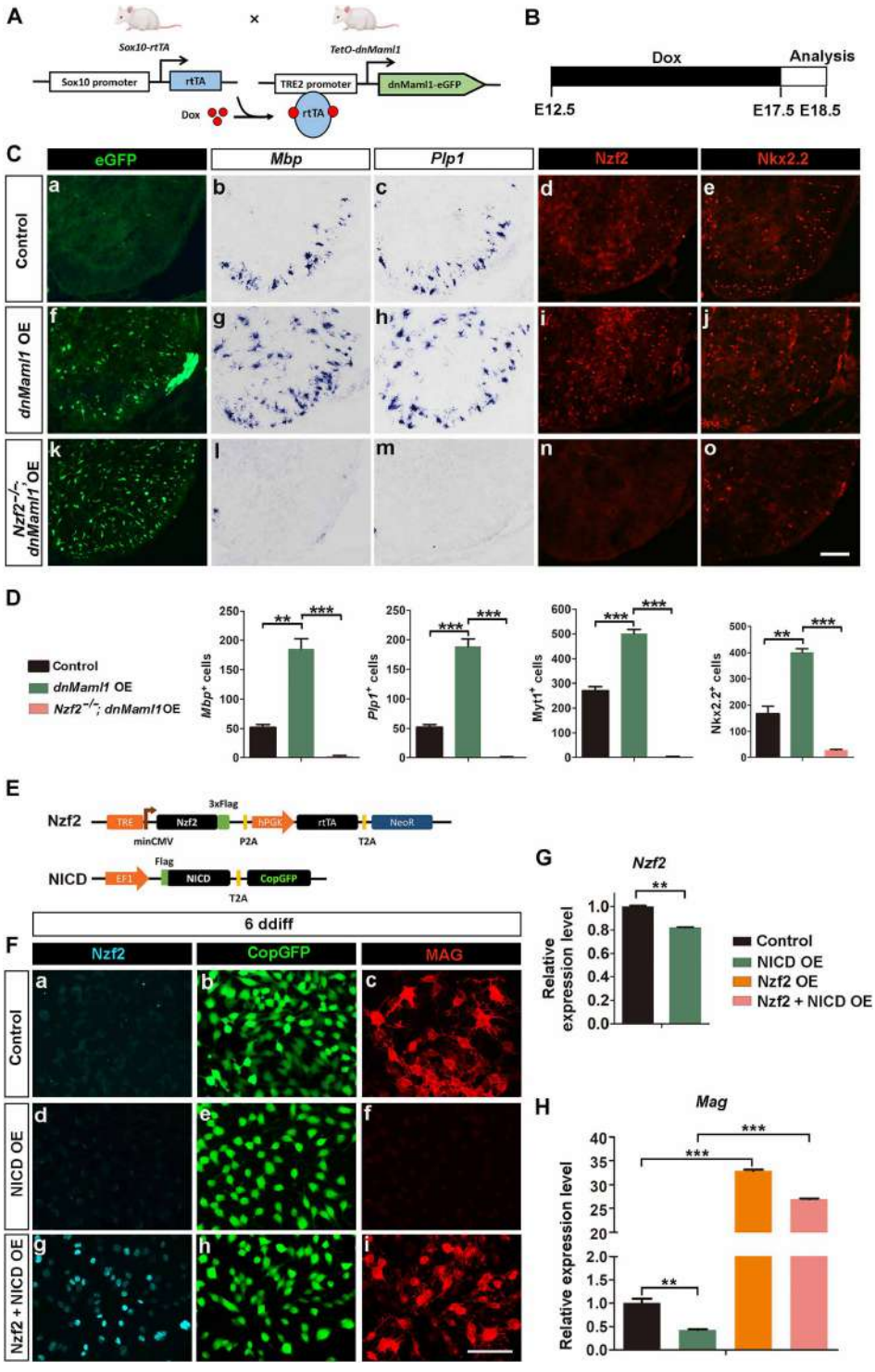

Fig. 8. Nzf2 functions downstream of Notch signaling to promote OL differentiation. (**A**) Schematic diagram of generation of *Sox10-rtTA*; *TetO-dnMaml1* mice to induce dnMaml1 overexpression in OPCs by Dox treatment. (**B**) Time window of Dox treatment. (**C**) ISH of *Mbp* and *Plp1* and immunostaining of Nzf2 and Nkx2.2 in the spinal cords of control, *dnMaml1* OE (*Sox10-rtTA*; *TetO-dnMaml1*), and *Nzf2*$^{-/-}$; *dnMaml1* OE mice at E18.5. (**D**) Quantification of *Mbp*-positive, *Plp1*-positive, Nzf2-positive, and Nkx2.2-positive cells per section in the spinal cords of control, *dnMaml1* OE (*Sox10-rtTA*; *TetO-dnMaml1*), and *Nzf2*$^{-/-}$; *dnMaml1* OE mice at E18.5 from (C). (**E**) Schematic diagram of Nzf2 and NICD overexpression constructs. (**F**) Double immunostaining of Nzf2 (blue) and MAG (red) in NICD-overexpressed CG4 cells at 6 ddiff, with or without Dox treatment. (**G**) qRT-PCR analysis of *Nzf2* expression levels in control and NICD-overexpressed CG4 cells at 6 ddiff from (F). (**H**) qRT-PCR analysis of *Mag* expression levels in control, NICD-overexpressed, Nzf2-overexpressed, and co-overexpressed CG4 cells at 6 ddiff from (F). Errors bars indicated SEM. $^{**}P \leq 0.005$ and $^{***}P \leq 0.001$. Scale bars, 100 μm.

orchestrated by the Notch-Nzf2-Nkx2.2 axis that governs OL differentiation (Fig. 9). In undifferentiated, immature OPCs, the activation of Notch signaling acts as a checkpoint, suppressing Nzf2 expression. Concurrently, histone deacetylation represses the transcription of *Nkx2.2*. However, upon deactivation of Notch signaling at later stages of OPC development, the repression of Nzf2 is alleviated. In the presence of Nzf2, it specifically recognizes and binds to the AAG/CTT motif throughout the genome and physically interacts with nearby HDAC1, preventing the assembly of functional repressor complexes. Consequently, histone acetylation of target genes is enhanced, enabling the transcriptional activation of *Nkx2.2*. This orchestrated process ultimately triggers and drives the differentiation of OPCs into OLs.

Nzf2 controls the timing of OL differentiation through activating Nkx2.2 expression

The proper formation of myelin sheaths around axons depends on the timely differentiation of OLs, which occurs on a predictable schedule both during development and in culture. A long-standing hypothesis posits the existence of an internal "clock" that gauges the duration and number of cell divisions in OPCs (*15*, *49*). However, the precise timing mechanism governing OL differentiation during normal development is still not fully understood. Earlier studies have indicated the Nkx2.2 transcription factor as a pivotal timing element in the orchestration of OL differentiation. In the developing rodent spinal cord, Nkx2.2 expression is transiently up-regulated in OPCs during the differentiation period (*20*, *22*). Overexpression of Nkx2.2 in OPCs leads to precocious OL differentiation (*21*), whereas conditional ablation of *Nkx2.2* results in a temporal delay in OL differentiation (*22*). A more recent study demonstrated that Nkx2.2 controls the timing of OL differentiation by directly suppressing the expression of PDGFRα in OPCs (*21*), potentially through the recruitment of a repressor complex that includes HDACs and the DNA methyltransferase Dnmt3a (*50*). Given that PDGFRα signaling promotes OPC proliferation but inhibits OL differentiation (*51*, *52*), Nkx2.2 emerges as a crucial cell-intrinsic factor that activates the differentiation program in OLs. Despite these insights, the upstream regulators of Nkx2.2 expression have remained elusive until now.

In this study, we provided several lines of evidence that Nzf2 functions upstream of Nkx2.2 in controlling the timing of OL differentiation. First, in the developing CNS, both Nzf2 and Nkx2.2 are transiently expressed in differentiating OPCs and NFOs, with Nzf2 expression being slightly earlier than that of Nkx2.2 (Fig. 5A). Second, genetic ablation of *Nzf2* completely abolishes Nkx2.2 expression during the OL differentiation stage (Fig. 5B), whereas overexpression of Nzf2 in CG4 cells significantly elevates the expression of Nkx2.2 which does not appear to directly activate myelin gene expression (Fig. 5E). Third, misexpression of Nzf2 and Nkx2.2 has a

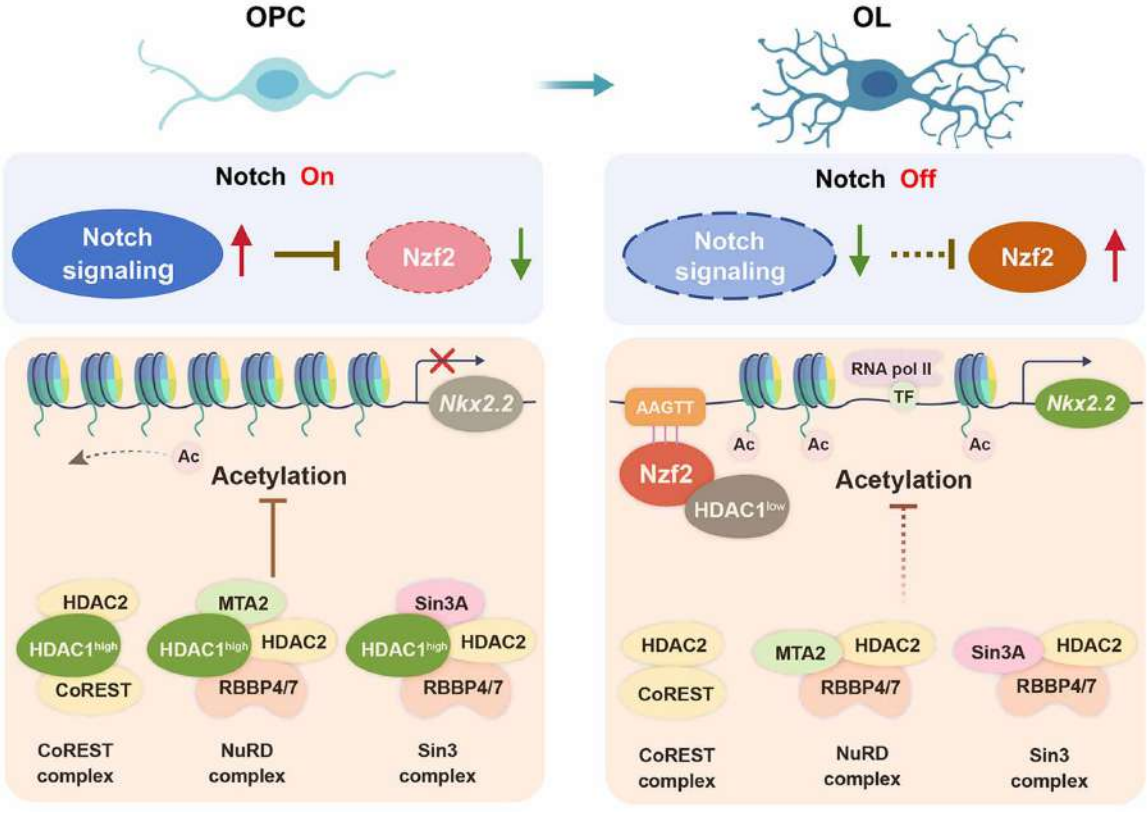

Fig. 9. Schematic diagram of the intricate cascade of the Notch-Nzf2-Nkx2.2 axis that initiates OL differentiation. In undifferentiated OPCs, Notch signaling functions to inhibit Nzf2 expression. Concurrently, the expression of prodifferentiation factor Nkx2.2 is inhibited under histone deacetylation. Upon deactivation of Notch signaling in late OPCs, the repression of Nzf2 is alleviated. Nzf2 specifically recognizes and binds to the AAG/CTT motif across genomes and physically interacts with nearby HDAC1, thus preventing the assembly of functional repressor complexes and subsequently elevating histone acetylation levels of Nkx2.2. In this way, Nkx2.2 initiates expression and drives OL differentiation.

similar effect on the timing of OPC differentiation both in vivo and in vitro (Fig. 5M). Fourth, ChIP-seq analysis and EMSA revealed that Nzf2 is able to directly bind to the *Nkx2.2* genome via the AAG/CTT motif (Fig. 5, G and J). Last and directly, induced expression of Nkx2.2 in *Nzf2*-deficient OPCs at least partially rescues the OL differentiation defects (Fig. 5M). On the basis of these observations, we propose that Nkx2.2 is a direct downstream mediator of Nzf2 in initiating an OL differentiation process.

Nzf2 epigenetically activates Nkx2.2 expression through blocking the assembly of HDAC1 repressor complexes

A variety of zinc finger proteins cooperate with chromatin modifiers to delicately control the transcription of target gene during development (*32*–*35*). Epigenetic chromatin remodeling events such as histone modification are essential for many biological processes, including OL development (*40*). Previous experiments have demonstrated that deacetylation of histone H3 by HDACs regulates OPC differentiation and maturation (*38*). Valproic acid (VPA), a HDAC inhibitor, was recently shown to have positive effects on OL generation and function (*53*, *54*). Treatment of neural stem cells (NSCs) with VPA promoted OL differentiation. The exact molecular mechanism underlying the HDAC inhibition of OL differentiation remains unsolved. In the present study, we identified Nzf2 as a previously unknown HDAC1 inhibitor expressed in differentiating OPCs, as it physically interacts with HDAC1 (Fig. 6, G and I) and hinders its repressor complex assembly (Fig. 6J). The interaction between Nzf2 and HDAC1 diminishes the deacetylase activity of HDAC1 (Fig. 6M). Consistently, a strong enrichment of Nzf2 in its downstream gene *Nkx2.2* is marked by H3K9ac and H3K27ac modifications (Fig. 6A). Moreover, transcription of *Nkx2.2* gene is regulated by histone acetylation, and treatment of CG4 cells with TSA, another HDAC inhibitor, increased *Nkx2.2* transcription and promoted OL differentiation and maturation (fig. S5, E and F). On the contrary, overexpression of HDAC1 protein inhibited CG4 cell differentiation (Fig. 6P). Collectively, our findings indicated that Nzf2 activates Nkx2.2 expression by inhibiting its histone deacetylation, resulting in increased acetylation and open chromatin structure for target gene transcription (Fig. 9).

Nzf2 functions downstream of the Notch signaling pathway in regulating OL differentiation

Previous studies have suggested that the canonical Notch signaling pathway is a key regulator of OL differentiation (*23*). Ablation of *Notch1* or its downstream *Hes5* in OL lineage cells resulted in a mild increase in myelin gene expression in the developing CNS (*55*–*57*). Conversely, overexpression of Notch1 and Hes5 or activation of Notch signaling by Jagged or Delta ligands led to an inhibition of OL differentiation in vitro (*58*, *59*). More recently, we demonstrated that inhibition of pan-Notch signaling by *dnMaml1* caused robust precocious OL differentiation and axonal myelination (*24*). Although these studies clearly demonstrated that Notch signaling is a critical and developmentally relevant inhibitor of OL differentiation, its primary downstream targets regulating OL differentiation have remained elusive.

The phenotype of precocious OL differentiation after *Nzf2* or *Nkx2.2* overexpression closely resembles that observed in *dnMaml1* transgenic mice, raising the possibility that dnMaml1 functions upstream of the Nzf2-Nkx2.2 axis. In support of this notion, we found that expression of both Nzf2 and Nkx2.2 was up-regulated markedly upon dnMaml1 overexpression in OPCs (Fig. 8C). Deletion of *Nzf2* blocked dnMaml1 induction of precocious OL differentiation and myelin gene expression in transgenic mice (Fig. 8C). Conversely, Nzf2 overexpression mitigated the inhibitory effect of NICD on OL differentiation (Fig. 8F). Together, these results strongly suggest that Nzf2 is a key downstream effector of the Notch signaling pathway in governing OL differentiation and myelin gene expression. It is conceivable that Notch signaling in immature OPCs functions to repress Nzf2 expression and cell differentiation, and diminished Notch signaling at later stages derepresses Nzf2 expression which in turn activates Nkx2.2 expression and initiates OL differentiation (Fig. 9). Accordingly, we propose that the Notch-Nzf2-Nkx2.2 axis constitutes the crucial regulatory pathway in the control of the timing of OL differentiation and myelin development.

MATERIALS AND METHODS

Animal procedures

All research protocols using animals were approved by the Institutional Animal Care and Use Committee at Hangzhou Normal University (approval number: HSD20211210). All mice were bred in specific pathogen–free facilities under a C56BL/6 background. Mice were kept under standard housing conditions with 12-hour light/12-hour dark cycle with free access to water and food. Both sexes were equally used in all experiments to ensure claims included data from both male and female mice. However, we cannot make any direct claims about the influences of sex on our findings as we are underpowered for most of our analyses based on sex. The *Nzf2*/*Myt1* conventional KO ($Nzf2^{+/-}$) mice were obtained from Mutant Mouse Resource & Research Centers supported by National Institutes of Health (stock no. 030295-UNC). For generation of the *Nzf2* cKO line, $Nzf2^{flox}$ mice (Shanghai Biomodel Organism) were designed to delete axons 8 and 9 in the mouse *Nzf2* gene (fig. S2A) and mated with the $Olig1^{cre}$ knock-in line (*60*). For generation of the *R26-Nkx2.2* mouse line, full length of the *Nkx2.2* open reading frame was cloned into the *Gt(ROSA)26Sor* locus. Expression of ectopic Nkx2.2 was blocked by a loxP-flanked STOP fragment placed between the *Gt(ROSA)26Sor* promoter and the *Nkx2.2* coding sequence. The time- and cell-specific overexpression of Nkx2.2 was achieved by crossing the *R26-Nkx2.2* mouse line with the *PDGFRα-creERT2* strain obtained from the Jackson Laboratory (stock no. 018280). *TetO-dnMaml1* transgenic mice were obtained from the Jackson Laboratory (stock no. 017918) and mated with the *Sox10-rtTA* knock-in mouse line (*61*) to produce *Sox10-rtTA*; *TetO-dnMaml1* double transgenic mice. Genotyping was performed by PCR using genomic DNA extracted from ear or toe biopsies. Primers used for genotyping are listed in table S5.

Fertilized chicken eggs (Chunpai Agricultural Technology Co. Ltd, Ningbo, China) were incubated at 37.5°C in a humidified incubator for 48 hours and windowed to reveal the embryos. Chicken embryos were staged according to the criteria set by Hamburger and Hamilton (*62*).

Immunofluorescence staining

For immunostaining, antibodies against Nzf2 (Oasis Biofarm, catalog no. OB-PRB015), Olig2 (Oasis Biofarm, catalog no. OB-PGP040), Sox10 (Oasis Biofarm, catalog no. OB-PGP001), Myrf (Oasis Biofarm, catalog no. OB-PRT003), CC1 (Oasis Biofarm, catalog no. OB-PRT039), ASPA (Oasis Biofarm, catalog no. OB-PRT005), NeuN (Millipore, catalog no. MAB377), GFAP (Millipore, catalog no. MAB360), Flag

(Sigma-Aldrich, catalog no. F1804), Nkx2.2 (Developmental Studies Hybridoma Bank, DSHB, catalog no. 74.5A5), MBP (Abcam, catalog no. ab7349), and Plp1 (Oasis Biofarm, catalog no. OB-PRT040) were used. *Nzf2*$^{-/-}$ and littermate control mice at defined stages were deeply anesthetized and perfused with ice-cold phosphate-buffered saline (PBS) and then 4% paraformaldehyde (PFA). Spinal cords were isolated and postfixed in 4% PFA overnight at 4°C and then transferred into 30% sucrose in PBS overnight at 4°C. Tissues were then embedded in optimal cutting temperature compound (Sakura Finetek) and sectioned on a cryostat with 14- to 16-μm thickness. Immunostaining was carried out as previously described (*63*) with minor modifications. Cryosections were blocked in blocking buffer (5% goat serum and 0.2% Triton X-100 in PBS) for 1 hour at room temperature and then incubated with primary antibodies overnight at 4°C. After washing three times with PBS, sections were incubated at room temperature for 1 hour with Alexa Fluor 488 or Alexa Fluor 594 secondary antibodies (Invitrogen). Nuclear labeling was completed by incubating slices with 4′,6-diamidino-2-phenylindole for 5 min. Images were taken by a Leica DMI600B inverted microscope. The antibodies and antiserum used were listed in table S6. All experiments were independently repeated at least three times.

RNA ISH

RNA ISH was carried out as previously described (*64*). Spinal cord sections mounted on microscope slides were hybridized with digoxigenin (DIG)–labeled probes in a humidified and sealed container at 60°C overnight. DIG-labeled RNA probes were generated by in vitro transcription with the T3/T7 RNA polymerase (Promega, catalog no. P2803/P2077), diluted with hybridization buffer and denatured at 85°C before use. After overnight hybridization, sections were rinsed in wash buffer and then incubated in blocking buffer (10% heat-inactivated sheep serum) for 1 hour at room temperature. Tissue slides were then incubated with anti–DIG–alkaline phosphatase antibody (Roche, catalog no. 11093274910) overnight at 4°C. The color reaction was performed using the NBT (nitro-blue-tetrazolium)-BCIP (5-bromo-4-chloro-3-indolyl-phosphate) kit (Roche, catalog no. 11681451001). Images were taken by a Nikon Eclipse 90i microscope.

Cell culture

HEK293T cells [American Type Culture Collection (ATCC), RRID: CVCL_0045] were routinely cultured in Dulbecco's modified Eagle's medium (DMEM) (CellMax, catalog no. CGM102.05) supplemented with 10% fetal bovine serum (FBS) (Biological Industries, catalog no. 04-001-01A) and penicillin-streptomycin (1000 U/ml; Gibco, catalog no. 15140148) in a humidified incubator with 5% CO_2 at 37°C. Rat CG4 cells (ATCC, RRID: CVCL_0210) were plated into a poly-L-lysine–coated glass coverslips at a density of 10,000 cells/cm^2 with DMEM/F12 (Gibco, catalog no. C11330500BT) supplemented with N2 (Gibco, catalog no. A1370701), B27 (Gibco, catalog no. A17504044), and PDGF-AA (10 ng/ml; PeproTech, catalog no. 100-13A). For differentiation induction, the medium was replaced with DMEM/F12 medium with N2, B27, and T3 (40 ng/ml; Sigma-Aldrich, catalog no. T6397). All cells were kept up with replacement of the medium every 2 days.

Tamoxifen and Dox treatment

Tamoxifen (Sigma-Aldrich, catalog no. T5648) was dissolved in corn oil at a concentration of 20 mg/ml. To induce Nkx2.2 overexpression in OPCs, tamoxifen was administered to pregnant female *R26Nkx2.2*; *PDGFRα-creERT2* mice through intraperitoneal injection at a dosage of 40 μg/g (grams, body weight). To induce dnMaml1 overexpression in OPCs, Dox (Sigma-Aldrich, catalog no. 10592-13-9) was administered at indicated stages both in the drinking water (4 mg/ml) and food (Bio-Serv). Single transgenic *Sox10-rtTA* and double transgenic *Sox10-rtTA*; *TetO-dnMaml1* mice of either sex were treated with Dox. For Nzf2 overexpression in CG4 cells, Dox was added into the medium with a final concentration of 2.5 μg/ml.

Viral production and cell transfection

The full-length fragments encoding mouse Nzf2 and 3×Flag were amplified and cloned into the pCW57-MCS1-P2A-MCS2 (neo) (Addgene, catalog no. 89180) vector. According to published studies (*65*), the encoding sequences of intracellular domain of mouse Notch1 were amplified and cloned into the pCDH-EF1-MCS-T2A-CopGFP (System Biosciences, catalog no. CD521A-1) vector. The full-length fragments encoding mouse HDAC1 were amplified and cloned into the pCDH-CMV-MCS-TSA-mCherry vector. All the constructs were confirmed by DNA sequencing. For lentivirus production, pCW57-Nzf2 was mixed with psPax2 (Addgene, catalog no. 12260) and pMD2.G (Addgene, catalog no. 12259) (4:3:1) to transfect HEK293T cells. After 48 hours, the medium with lentivirus was filtered through 0.45-μm filters, and high-titer lentiviruses were generated as described previously (*66*). CG4 cells infected with the pCW57-Nzf2 virus were further screened with G418 (100 μg/ml; Sango Biotech, catalog no. A600958) to obtain stable Nzf2 overexpression clones. For Nzf2 and NICD or HDAC1 co-overexpression, the stable Nzf2-overexpressed CG4 cells were reinfected with pCDH-NICD or pCDH-HDAC1 viruses.

Western blotting

Western blotting was performed as previously described (*67*). Brain tissues from deeply anesthetized *Nzf2*$^{-/-}$ and littermate control mice at P0 were dissected and homogenized. The samples were lysed overnight at 4°C in a lysis buffer [25 mM tris-HCl (pH 7.4), 150 mM NaCl, 1% NP-40, 0.5% Triton X-100, and 1 mM EDTA] supplemented with protease inhibitor cocktail (Sigma-Aldrich, catalog no. P0044). For cell cultures, each well of six-well plates was rinsed with PBS and lysed in a chilled lysis buffer for 30 min on ice. Lysates were centrifuged at 12,000*g* for 15 min at 4°C. Concentration of the supernatant was measured by the Bicinchoninic Acid (BCA) assay. A total of 20 μg of protein was loaded onto a SDS–polyacrylamide gel electrophoresis gel and then transferred to a polyvinylidene difluoride membrane (Millipore, catalog no. ISEQ00010). The membrane was blocked by 5% nonfat milk solution in tris-buffered saline with Tween-20 (TBST) for 1 hour at room temperature and then incubated with primary antibodies overnight at 4°C. Next day, the membranes were washed three times with TBST and incubated with horseradish peroxidase–conjugated secondary antibodies for 1 hour at room temperature. Proteins were detected using an enhanced chemiluminescence detection system (Thermo Fisher Scientific, catalog no. 32109) and an x-ray film.

Spinal cord explant culture

Segments of spinal cord tissues at the thoracic region were dissected from wild-type and *Nzf2*$^{-/-}$ embryos at E14.5 and grown on 8-μm nucleopore polycarbonate membranes (Costar), floating on the culture medium containing DMEM/F12, 20% FBS, and penicillin-streptomycin

(1000 U/ml) at 37°C in a humidified incubator with 5% CO_2. After 7 days of culture in vitro, explants were then fixed in 4% PFA and processed for whole-mount ISH with *Mbp* RNA probes, as described previously (*68*).

In ovo electroporation

For Nzf2 overexpression in chick embryos, the full-length fragments encoding mouse Nzf2 tagged with Flag at the N terminus were amplified and cloned into PB (piggyBac) retrovirus vectors to construct the PB-Flag-Nzf2-P2A-nlsCopGFP plasmid. The procedure for in ovo electroporation has been described previously (*69*). Briefly, the DNA mixture containing the PB-Flag-Nzf2-P2A-nlsCopGFP plasmid (2.5 μg/μl), PBase (1 μg/μl; PB transposase helper plasmid), and 1% fast green (MedChem Express, catalog no. HY-D0914) was injected into the central lumen of chick spinal cords at cE2 with a glass capillary. Square-wave current (five pulses, 20 V, 50 ms per pulse) was generated using a BTX Electro Square Porator T820. Embryos were then incubated in a humidified incubator at 37°C and harvested at cE7 and cE9. Segments of spinal cords with high levels of the copGFP signal were dissected and fixed in 4% PFA for further analysis.

TUNEL assay

Apoptosis detection was conducted according to the instruction of the DeadEnd Fluorometric TUNEL system (Promega, catalog no. G3250). The tissue sections were postfixed in 4% PFA, followed by treatment with proteinase K (20 μg/ml) to ensure proper adherence. Subsequently, sections were rinsed in equilibration buffer for 10 min at room temperature and then incubated in the terminal deoxynucleotidyl transferase (TdT) reaction mix for 60 min at 37°C. The reaction was terminated using 2× SSC. After rinsing the sections three times in PBS, the sections were subjected to subsequent immunofluorescence staining analysis.

Real-time quantitative polymerase chain reaction

Total RNA was harvested from cells and spinal cord tissues using the TRIzol Reagent (Invitrogen, catalog no. 15596026) according to the manufacturer's instructions, and genomic DNA was removed using deoxyribonuclease I (Takara, catalog no. 2270A). The first-strand cDNA was synthesized from 1 μg of the total RNA using the HiScript III First Strand cDNA Synthesis Kit (Vazyme, catalog no. R312). The quantitative PCR experiments were conducted using ChamQ Universal SYBR MasterMix (Vazyme, catalog no. Q711-02) according to the manufacturer's instructions. Primer sequences used in this study were listed in table S7. All reactions were performed in triplicate with three independent experiments, and the relative expression levels were calculated using the $2^{-\Delta\Delta Ct}$ method.

LPC injection

Focal demyelination insults were performed in the corpus callosum of 8-week-old wild-type mice. Two microliters of 1% LPC (Sigma-Aldrich, catalog no. L1381) was injected into corpus callosum (Anterior-Posterior, AP: 0.80 mm; Medial-Lateral, ML: 0.1 mm; Dorsal-Ventral, DV: 0.22 mm relative to bregma). Mice were allowed to recover and euthanized at 7 and 10 dpl.

TrueGold myelin staining

After returning to room temperature, the cryosections were baked at 37 °C for 30 min. The TrueGold myelin staining solution (Oasis Biofarm, catalog no. BK-AC001) was added to the sections and incubated at 45°C for 20 to 30 min. The slides were then rinsed twice with deionized water, followed by thiosulfate solution, and incubated at 45°C for 3 min. Last, the slides were cover-slipped with mounting medium for bright-field microscope observation.

Single-cell RNA-seq and data analysis

Procedures of cell isolation, RNA capture, reverse transcription, and single-cell sequencing were executed by Hangzhou Lianchuan Biotechnology Co. Ltd. (Hangzhou, China). Spinal tissues were dissected from wild-type C57BL/6 mice at E15.5, P4, and P15, promptly immersed in ice-cold Hanks' balanced salt solution (Gibco, catalog no. 12175-095) to preserve cellular integrity. Using the Papain Cell Dissociation Kit (Miltenyi Biotec, catalog no. 130-092-628), these tissues were gently dissociated into single-cell suspensions. Subsequently, the Chromium droplet-based sequencing platform from 10x Genomics was used to generate scRNA-seq libraries. The cDNA libraries underwent purification and quantification using the Agilent 2100 Bioanalyzer, facilitating sequencing on an Illumina Hiseq4000 platform. The resulting sequences (clean reads) were processed with Cell Ranger to obtain quantitative gene expression profiles. Cellular quality control thresholds were set at 500 to 5000 genes and <10% mitochondrial transcripts per cell. After filtering, 30,511 single cells were successfully captured and sequenced. To facilitate data visualization, we used the Seurat package (v4.1.0) for dimensionality reduction. Gene expression values were normalized using the LogNormalize method, followed by principal components analysis leveraging the top 10 principal components to guide clustering and UMAP analysis. Clusters were identified using the weighted shared nearest neighbor graph–based clustering approach, with marker genes for each cluster determined through the Wilcoxon rank sum test, using default parameters ("bimod": likelihood ratio test) within the FindAllMarkers function of Seurat. For cluster annotation, we searched for the most comprehensive and reliable cell type markers according to published papers (*2*, *28*). For the comprehensive analysis of the resultant single-cell data, we leveraged the OmicStudio tools, developed by LC-BIO Co. Ltd. (Hangzhou, China), accessible at www.omicstudio.cn/cell.

RNA-seq and data analysis

RNA purification, reverse transcription, library construction, and sequencing were performed at Shanghai Majorbio Bio-pharm Biotechnology Co. Ltd (Shanghai, China). The transcriptome library was prepared following the TruSeq RNA Sample Preparation Kit from Illumina (San Diego, CA) using 1 μg of the total RNA. Sequencing was performed with the Illumina NovaSeq 6000 sequencer (2 × 150–bp read length). To identify DEGs (differentially expressed genes) upon Nzf2 deletion, the expression level of each gene was calculated according to the transcripts per million reads method. RNA-Seq by Expectation-Maximization (RSEM) (http://deweylab.biostat.wisc.edu/rsem/) was used to quantify gene abundance. Differential expression analysis was performed using DESeq2, and DEGs with $\log_2$ fold ≥ 1 and adjusted $P \leq 0.05$ are considered to be significant DEGs. GO analysis was performed to identify which DEGs were significantly enriched in GO terms compared with the whole-transcriptome background and carried out by Goatools (http://github.com/tanghaibao/Goatools).

ChIP-seq, ATAC-seq, and data analysis

ChIP was performed in CG4 cells using the SimpleChIP Enzymatic Chromatin IP Kit (magnetic beads) (Cell Signaling Technology, CST, catalog no. 9003) according to the manufacturer's instructions. Our anti-Nzf2 antibody was used for IP experiments. Briefly, Dox-treated CG4 cells were cross-linked with 1% paraformaldehyde at room temperature, and chromatin was sheared to a fragment of 150 to 400 bp with a Scientz-IID sonicator. A total of 10% of the sheared chromatin sample was removed as the input group. Antibodies including rabbit anti-Nzf2, normal rabbit immunoglobulin G (negative control), and histone H3 (D2B12) XP Rabbit monoclonal antibody (positive control) were added to chromatin and incubated overnight at 4°C. Chromatin-protein complex was immunoprecipitated with protein G magnetic beads. Then, cross-linking was reversed via incubation at 65°C for 30 min with proteinase K digestion, and DNA was purified with the NucleoSpin Gel and the PCR clean-up Kit. Eluted DNA was then used for quantitative PCR, and the $2^{-\Delta\Delta Ct}$ method was used to calculate the percent recovery of a specific DNA region from the total input. The primers used for ChIP-qPCR were shown in table S7. Each experiment was performed in three biological replicates.

ATAC-seq was performed from spinal cord tissues of neonatal wild-type and *Nzf2*$^{-/-}$ mice. Spinal cord tissues were dissected and washed with cold PBS. After grinding and filtering, the filtrate was centrifuged at 500*g* for 5 min at 4°C, and then the supernatant was discarded. After density gradient centrifugation for 10 min, nuclear suspension was obtained. The nucleus pellet was resuspended in the Tn5 transposase reaction mix and incubated at 37°C for 30 min. Equimolar adapter 1 and adapter 2 were added after transposition, and PCR was then performed to amplify the library.

Library construction and sequencing of ChIP-seq and ATAC-seq were performed by Novogene Co. Ltd. (Beijing, China). Pair-end sequencing was performed on the Illumina platform (San Diego, CA). Library quality was assessed on the Agilent Bioanalyzer 2100 system. Data were processed further with Model-based Analysis of ChIP-Seq (MACS) version 2.1.0 peak-calling software to identify regions enriched in IP over input samples. A *q* value threshold of 0.05 was used for all datasets. HOMER was used to detect the de novo motif and the matched known motifs of Nzf2 peaks.

Co-IP assay

For the co-IP assay, HEK293T cells were transiently transfected with Nzf2-3×Flag and HDAC1-3×HA or GCN5. Forty-eight hours after transfection, HEK293T cells were washed with PBS and lysed in a 1.5-ml lysis buffer containing 50 mM tris (pH 7.4), 150 mM NaCl, 1% Triton X-100, 1 mM EDTA, and protease inhibitor cocktail (Sigma-Aldrich, catalog no. P8340) at 4°C for 20 min. The cell lysate was spun down at 13,000*g* for 10 min at 4°C. Two hundred microliters of lysate was used as an input sample. The left was added into a 2.5-ml lysis buffer and filtered with a 0.22-μm strainer. The cleared lysate was mixed with 40-μl anti-Flag magnetic beads (Sigma-Aldrich, catalog no. M8823) and incubated overnight at 4°C. Then, beads were washed with a lysis buffer three times. Proteins bound to the beads were eluted with 300 μl of tris-buffered saline containing 20-μg 3×FLAG peptides at room temperature for 30 min. Twenty-microliter input/IP samples were used for Western blot.

Electrophoretic mobility shift assay

EMSA was performed using 3′-end biotin-labeled probes for the putative Nzf2-binding sites (positions −996 to −1040) in the *Nkx2.2* promoter region. Briefly, the probe was incubated with purified Nzf2 proteins for 30 min at room temperature. Other steps were performed according to the EMSA/Gel-shift Kit protocol (Beyotime, catalog no. GS002). For supershift experiments, a Nzf2-specific antibody was added to the assay.

HDAC activity assay

The HDAC activity assay was performed using the Histone Deacetylase Activity Assay Kit (Abcam, catalog no. ab156064) according to the manufacturer's instructions. Briefly, 10 μl of purified Nzf2 or GFAP proteins was mixed with HDAC assay buffer, substrate, and developer and then incubated at room temperature. Fluorescence intensity was measured every 5 min.

Statistical analysis

Results from independent animals, experiments, or separately generated samples were treated as biological replicates. The number of samples per group was $n \geq 3$ for all mice and molecular biology treatments except for ChIP-seq analysis. All data were analyzed using Prism GraphPad 9.0 and presented as mean ± SEM. An unpaired two-tailed Student's *t* test was used for analysis between two groups with one variable. Statistical significance was set at $^{*}P \leq 0.05$, $^{**}P \leq 0.01$, and $^{***}P \leq 0.001$.

Supplementary Materials

The PDF file includes:

Figs. S1 to S7

Legends for tables S1 to S7

Other Supplementary Material for this manuscript includes the following:

Tables S1 to S7

REFERENCES AND NOTES

1. D. E. Bergles, W. D. Richardson, Oligodendrocyte development and plasticity. *Cold Spring Harb. Perspect. Biol.* **8**, a020453 (2015).
2. S. Marques, A. Zeisel, S. Codeluppi, D. van Bruggen, A. M. Falcão, L. Xiao, H. Li, M. Häring, H. Hochgerner, R. A. Romanov, D. Gyllborg, A. M. Manchado, G. L. Manno, P. Lönnerberg, E. M. Floriddia, F. Rezayee, P. Ernfors, E. Arenas, J. Hjerling-Leffler, T. Harkany, W. D. Richardson, S. Linnarsson, G. Castelo-Branco, Oligodendrocyte heterogeneity in the mouse juvenile and adult central nervous system. *Science* **352**, 1326–1329 (2016).
3. M. Fang, L. Chen, T. Tang, M. Qiu, X. Xu, The committed oligodendrocyte precursor cell, a newly-defined intermediate progenitor cell type in oligodendroglial lineage. *Glia* **71**, 2499–2510 (2023).
4. F. Wang, S. Y. Ren, J. F. Chen, K. Liu, R. X. Li, Z. F. Li, B. Hu, J. Q. Niu, L. Xiao, J. R. Chan, F. Mei, Myelin degeneration and diminished myelin renewal contribute to age-related deficits in memory. *Nat. Neurosci.* **23**, 481–486 (2020).
5. C. M. Bacmeister, R. Huang, L. A. Osso, M. A. Thornton, L. Conant, A. R. Chavez, A. Poleg-Polsky, E. G. Huges, Motor learning drives dynamic patterns of intermittent myelination on learning-activated axons. *Nat. Neurosci.* **25**, 1300–1313 (2022).
6. B. D. Trapp, J. Peterson, R. M. Ransohoff, R. Rudick, S. Mörk, L. Bö, Axonal transection in the lesions of multiple sclerosis. *N. Engl. J. Med.* **338**, 278–285 (1998).
7. S. Mar, M. Noetzel, Axonal damage in leukodystrophies. *Pediatr. Neurol.* **42**, 239–242 (2010).
8. N. Scolding, R. Franklin, S. Stevens, C. H. Heldin, A. Compston, J. Newcombe, Oligodendrocyte progenitors are present in the normal adult human CNS and in the lesions of multiple sclerosis. *Brain* **121**, 2221–2228 (1998).
9. J. M. Levine, R. Reynolds, Activation and proliferation of endogenous oligodendrocyte precursor cells during ethidium bromide-induced demyelination. *Exp. Neurol.* **160**, 333–347 (1999).
10. A. Chang, A. Nishiyama, J. Peterson, J. Prineas, B. D. Trapp, NG2-positive oligodendrocyte progenitor cells in adult human brain and multiple sclerosis lesions. *J. Neurosci.* **20**, 6404–6412 (2000).

11. A. Chang, W. W. Tourtellotte, R. Rudick, B. D. Trapp, Premyelinating oligodendrocytes in chronic lesions of multiple sclerosis. *N. Engl. J. Med.* **346**, 165–173 (2002).
12. R. J. Franklin, Why does remyelination fail in multiple sclerosis? *Nat. Rev. Neurosci.* **3**, 705–714 (2002).
13. B. Emery, Q. R. Lu, Transcriptional and epigenetic regulation of oligodendrocyte development and myelination in the central nervous system. *Cold Spring Harb. Perspect. Biol.* **7**, a020461 (2015).
14. B. Elbaz, B. Popko, Molecular control of oligodendrocyte development. *Trends Neurosci.* **42**, 263–277 (2019).
15. H. Huang, X. F. Zhao, K. Zheng, M. Qiu, Regulation of the timing of oligodendrocyte differentiation: Mechanisms and perspectives. *Neurosci. Bull.* **29**, 155–164 (2013).
16. T. Kondo, M. Raff, Basic helix-loop-helix proteins and the timing of oligodendrocyte differentiation. *Development* **127**, 2989–2998 (2000).
17. Q. Zhou, G. Choi, D. J. Anderson, The bHLH transcription factor Olig2 promotes oligodendrocyte differentiation in collaboration with Nkx2.2. *Neuron* **31**, 791–807 (2001).
18. J. Wittstatt, S. Reiprich, M. Kuspert, Crazy little thing called Sox-New insights in oligodendroglial Sox protein function. *Int. J. Mol. Sci.* **20**, 2713 (2019).
19. B. Emery, D. Agalliu, J. D. Cahoy, T. A. Watkins, J. C. Dugas, S. B. Mulinyawe, A. Ibrahim, K. L. Ligon, D. H. Rowitch, B. A. Barres, Myelin gene regulatory factor is a critical transcriptional regulator required for CNS myelination. *Cell* **138**, 172–185 (2009).
20. X. Xu, J. Cai, H. Fu, R. Wu, Y. Qi, G. Modderman, R. Liu, M. Qiu, Selective expression of Nkx-2.2 transcription factor in chicken oligodendrocyte progenitors and implications for the embryonic origin of oligodendrocytes. *Mol. Cell. Neurosci.* **16**, 740–753 (2000).
21. Q. Zhu, X. Zhao, K. Zheng, H. Li, H. Huang, Z. Zhang, T. Mastracci, M. Wegner, Y. Chen, L. Sussel, M. Qiu, Genetic evidence that Nkx2.2 and Pdgfra are major determinants of the timing of oligodendrocyte differentiation in the developing CNS. *Development* **141**, 548–555 (2014).
22. Y. Qi, J. Cai, Y. Wu, R. Wu, J. Lee, H. Fu, M. Rao, L. Sussel, J. Rubenstein, M. Qiu, Control of oligodendrocyte differentiation by the Nkx2.2 homeodomain transcription factor. *Development* **128**, 2723–2733 (2001).
23. S. Wang, A. D. Sdrulla, G. diSibio, G. Bush, D. Nofziger, C. Hicks, G. Weinmaster, B. A. Barres, Notch receptor activation inhibits oligodendrocyte differentiation. *Neuron* **21**, 63–75 (1998).
24. X. Ge, G. Xiao, H. Huang, J. Du, Y. Tao, A. Yang, H. Wu, Z. Zhang, M. Qiu, Stage-dependent regulation of oligodendrocyte development and enhancement of myelin repair by dominant negative Master-mind 1 protein. *Glia* **67**, 1654–1666 (2019).
25. J. G. Kim, L. D. Hudson, Novel member of the zinc finger superfamily: A C2-HC finger that recognizes a glia-specific gene. *Mol. Cell. Biol.* **12**, 5632–5639 (1992).
26. Y. Jiang, V. C. Yu, F. Buchholz, S. O'Connell, S. J. Rhodes, C. Candeloro, Y. R. Xia, A. J. Lusis, M. G. Rosenfeld, A novel family of Cys-Cys, His-Cys zinc finger transcription factors expressed in developing nervous system and pituitary gland. *J. Biol. Chem.* **271**, 10723–10730 (1996).
27. K. S. Yee, V. C. Yu, Isolation and characterization of a novel member of the neural zinc finger factor/myelin transcription factor family with transcriptional repression activity. *J. Biol. Chem.* **273**, 5366–5374 (1998).
28. S. Marques, D. van Bruggen, D. P. Vanichkina, E. M. Floriddia, H. Munguba, L. Väremo, S. Giacomello, A. M. Falcão, M. Meijer, A. K. Björklund, J. Hjerling-Leffler, R. J. Taft, G. Castelo-Branco, Transcriptional convergence of oligodendrocyte lineage progenitors during development. *Dev. Cell* **46**, 504–517.e7 (2018).
29. F. F. Vasconcelos, A. Sessa, C. Laranjeira, A. A. S. F. Raposo, V. Teixeira, D. W. Hagey, D. M. Tomaz, J. Muhr, V. Broccoli, D. S. Castro, Myt1 counteracts the neural progenitor program to promote vertebrate neurogenesis. *Cell Rep.* **17**, 469–483 (2016).
30. S. Wang, J. Zhang, A. Zhao, S. Hipkens, M. A. Magnuson, G. Gu, Loss of Myt1 function partially compromises endocrine islet cell differentiation and pancreatic physiological function in the mouse. *Mech. Dev.* **124**, 898–910 (2007).
31. T. Kuhlmann, V. Miron, Q. Cui, C. Wegner, J. Antel, W. Brück, Differentiation block of oligodendroglial progenitor cells as a cause for remyelination failure in chronic multiple sclerosis. *Brain* **131**, 1749–1758 (2008).
32. S. Kwak, T. W. Kim, B. H. Kang, J. H. Kim, J. S. Lee, H. T. Lee, I. Y. Hwang, J. Shin, J. H. Lee, E. J. Cho, H. D. Youn, Zinc finger proteins orchestrate active gene silencing during embryonic stem cell differentiation. *Nucleic Acids Res.* **46**, 6592–6607 (2018).
33. D. Fuhrmann, H. P. Elsässer, Schwann cell Myc-interacting zinc-finger protein 1 without pox virus and zinc finger: Epigenetic implications in a peripheral neuropathy. *Neural Regen. Res.* **13**, 1534–1537 (2018).
34. Y. Ying, M. Wang, Y. Chen, M. Li, C. Ma, J. Zhang, X. Huang, M. Jia, J. Zeng, Y. Wang, L. Li, X. Wang, Q. Tao, X. S. Shu, Zinc finger protein 280C contributes to colorectal tumorigenesis by maintaining epigenetic repression at H3K27me3-marked loci. *Proc. Natl. Acad. Sci. U.S.A.* **119**, e2120633119 (2022).
35. B. Dehingia, M. Milewska, M. Janowski, A. Pękowska, CTCF shapes chromatin structure and gene expression in health and disease. *EMBO Rep.* **23**, e55146 (2022).
36. J. Liu, L. Magri, F. Zhang, N. O. Marsh, S. Albrecht, J. L. Huynh, J. Kaur, T. Kuhlmann, W. Zhang, P. A. Slesinger, P. Casaccia, Chromatin landscape defined by repressive histone methylation during oligodendrocyte differentiation. *J. Neurosci.* **7**, 352–365 (2016).
37. W. Wang, H. Cho, D. Kim, Y. Park, J. H. Moon, S. J. Lim, S. M. Yoon, M. McCane, S. A. Aicher, S. Kim, B. Emery, J. W. Lee, S. Lee, Y. Park, S. K. Lee, PRC2 acts as a critical timer that drives oligodendrocyte fate over astrocyte identity by repressing the Notch pathway. *Cell Rep.* **32**, 108147 (2020).
38. F. Ye, Y. Chen, T. Hoang, R. L. Montgomery, X. H. Zhao, H. Bu, T. Hu, M. M. Taketo, J. H. van Es, H. Clevers, J. Hsieh, R. Bassel-Duby, E. N. Olson, Q. R. Lu, HDAC1 and HDAC2 regulate oligodendrocyte differentiation by disrupting the beta-catenin-TCF interaction. *Nat. Neurosci.* **12**, 829–838 (2009).
39. J. Liu, P. Casaccia, Epigenetic regulation of oligodendrocyte identity. *Trends Neurosci.* **33**, 193–201 (2010).
40. A. Gregath, Q. R. Lu, Epigenetic modifications-insight into oligodendrocyte lineage progression, regeneration and disease. *FEBS Lett.* **592**, 1063–1078 (2018).
41. D. M. Vigushin, S. Ali, P. E. Pace, N. Mirsaidi, K. Ito, I. Adcock, R. C. Coombes, Trichostatin A is a histone deacetylase inhibitor with potent antitumor activity against breast cancer in vivo. *Clin. Cancer Res.* **7**, 971–976 (2001).
42. Q. Jin, L.-R. Yu, L. Wang, Z. Zhang, L. H. Kasper, J.-E. Lee, C. Wang, P. K. Brindle, S. Y. R. Dent, K. Ge, Distinct roles of GCN5/PCAF-mediated H3K9ac and CBP/p300-mediated H3K18/27ac in nuclear receptor transactivation. *EMBO J.* **30**, 249–262 (2011).
43. T. Hayakawa, J.-I. Nakayama, Physiological roles of class I HDAC complex and histone demethylase. *J. Biomed. Biotechnol.* **2011**, 129383 (2011).
44. C. J. Millard, L. Fairall, T. J. Ragan, C. G. Savva, J. W. R. Schwabe, The topology of chromatin-binding domains in the NuRD deacetylase complex. *Nucleic Acids Res.* **48**, 12972–12982 (2020).
45. T. Pierfelice, L. Alberi, N. Gaiano, Notch in the vertebrate nervous system: An old dog with new tricks. *Neuron* **69**, 840–855 (2011).
46. G. Xiao, J. Du, H. Wu, X. Ge, X. Xu, A. Yang, Y. Zhu, X. Hu, K. Zheng, Q. Zhu, M. Qiu, Differential inhibition of Sox10 functions by Notch-Hes pathway. *Cell. Mol. Neurobiol.* **40**, 653–662 (2020).
47. L. Wu, T. Sun, K. Kobayashi, P. Gao, J. D. Griffin, Identification of a family of mastermind-like transcriptional coactivators for mammalian notch receptor. *Mol. Cell. Biol.* **22**, 7688–7700 (2002).
48. C.-Y. Peng, H. Yajima, C. E. Burn, L. I. Zon, S. S. Sisodia, S. L. Pfaff, K. Sharma, Notch and MAML signaling drives Scl-dependent interneuron diversity in the spinal cord. *Neuron* **53**, 813–827 (2007).
49. S. Temple, M. C. Raff, Clonal analysis of oligodendrocyte development in culture: Evidence for a developmental clock that counts cell divisions. *Cell* **44**, 773–779 (1986).
50. J. B. Papizan, R. A. Singer, S.-I. Tschen, S. Dhawan, J. M. Friel, S. B. Hipkens, M. A. Magnuson, A. Bhushan, L. Sussel, Nkx2.2 repressor complex regulates islet β-cell specification and prevents β-to-α-cell reprogramming. *Genes Dev.* **25**, 2291–2305 (2011).
51. M. C. Raff, L. E. Lillien, W. D. Richardson, J. F. Burne, M. D. Noble, Platelet-derived growth factor from astrocytes drives the clock that times oligodendrocyte development in culture. *Nature* **333**, 562–565 (1988).
52. I. K. Hart, W. D. Richardson, S. R. Bolsover, M. C. Raff, PDGF and intracellular signaling in the timing of oligodendrocyte differentiation. *J. Cell. Biol.* **109**, 3411–3417 (1989).
53. X. S. Liu, M. Chopp, H. Kassis, L. F. Jia, A. Hozeska-Solgot, R. L. Zhang, C. Chen, Y. S. Cui, Z. G. Zhang, Valproic acid increases white matter repair and neurogenesis after stroke. *Neuroscience* **220**, 313–321 (2012).
54. G. Castelo-Branco, T. Lilja, K. Wallenborg, A. M. Falcão, S. C. Marques, A. Gracias, D. Solum, R. Paap, J. Walfridsson, A. I. Teixeira, M. G. Rosenfeld, K. Jepsen, O. Hermanson, Neural stem cell differentiation is dictated by distinct actions of nuclear receptor corepressors and histone deacetylases. *Stem Cell Reports* **3**, 502–515 (2014).
55. A. Liu, J. Li, M. Marin-Husstege, R. Kageyama, Y. Fan, C. Gelinas, P. Casaccia-Bonnefil, A molecular insight of Hes5-dependent inhibition of myelin gene expression: Old partners and new players. *EMBO J.* **25**, 4833–4842 (2006).
56. S. Genoud, C. Lappe-Siefke, S. Goebbels, F. Radtke, M. Aguet, S. S. Scherer, U. Suter, K.-A. Nave, N. Mantei, Notch1 control of oligodendrocyte differentiation in the spinal cord. *J. Cell. Biol.* **158**, 709–718 (2002).
57. M. I. Givogri, R. M. Costa, V. Schonmann, A. J. Silva, A. T. Campagnoni, E. R. Bongarzone, Central nervous system myelination in mice with deficient expression of Notch1 receptor. *J. Neurosci. Res.* **67**, 309–320 (2002).
58. H.-C. Park, B. Appel, Delta-Notch signaling regulates oligodendrocyte specification. *Development* **130**, 3747–3755 (2003).
59. M. A. Rabadán, J. Cayuso, G. Le Dréau, C. Cruz, M. Barzi, S. Pons, J. Briscoe, E. Martí, Jagged2 controls the generation of motor neuron and oligodendrocyte progenitors in the ventral spinal cord. *Cell Death Differ.* **19**, 209–219 (2012).
60. Q. R. Lu, T. Sun, Z. Zhu, N. Ma, M. Garcia, C. D. Stiles, D. H. Rowitch, Common developmental requirement for Olig function indicates a motor neuron/oligodendrocyte connection. *Cell* **109**, 75–86 (2002).
61. A. Ludwig, B. Schlierf, A. Schardt, K. A. Nave, M. Wegner, Sox10-rtTA mouse line for tetracycline-inducible expression of transgenes in neural crest cells and oligodendrocytes. *Genesis* **40**, 171–175 (2004).

62. V. Hamburger, H. L. Hamilton, A series of normal stages in the development of the chick embryo. *Dev. Dyn.* **195**, 231–272 (1992).
63. X. Xu, Q. Yu, M. Fang, M. Yi, A. Yang, B. Xie, J. Yang, Z. Zhang, Z. Dai, M. Qiu, Stage-specific regulation of oligodendrocyte development by Hedgehog signaling in the spinal cord. *Glia* **68**, 422–434 (2020).
64. M. Fang, Q. Yu, B. Ou, H. Huang, M. Yi, B. Xie, A. Yang, M. Qiu, X. Xu, Genetic evidence that dorsal spinal oligodendrocyte progenitor cells are capable of myelinating ventral axons effectively in mice. *Neurosci. Bull.* **36**, 1474–1483 (2020).
65. N. Gaiano, J. S. Nye, G. Fishell, Radial glial identity is promoted by Notch1 signaling in the murine forebrain. *Neuron* **26**, 395–404 (2000).
66. Z. M. Dai, W. Guo, D. Yu, X. J. Zhu, S. Sun, H. Huang, M. Jiang, B. Xie, Z. Zhang, M. Qiu, SECISBP2L-mediated selenoprotein synthesis is essential for autonomous regulation of oligodendrocyte differentiation. *J. Neurosci.* **42**, 5860–5869 (2022).
67. H. Huang, P. Teng, J. Du, J. Meng, X. Hu, T. Tang, Z. Zhang, Y. B. Qi, M. Qiu, Interactive repression of MYRF self-cleavage and activity in oligodendrocyte differentiation by TMEM98 protein. *J. Neurosci.* **38**, 9829–9839 (2018).
68. J. Cai, T. St Amand, H. Yin, H. Guo, G. Li, Y. Zhang, Y. Chen, M. Qiu, Expression and regulation of the chicken Nkx-6.2 homeobox gene suggest its possible involvement in the ventral neural patterning and cell fate specification. *Dev. Dyn.* **216**, 459–468 (1999).
69. X. Xu, Z. Liu, H. Huang, K. Zheng, X. Hu, Z. Zhang, M. Qiu, AP-2α and AP-2β regulate dorsal interneuron specification in the spinal cord. *Neuroscience* **340**, 232–242 (2017).

Acknowledgments
Funding: This work was partially supported by grants from Brain Initiative Grant of the Ministry of Science and Technology, China (STI2030-Major Projects 2022ZD0204700), National Natural Science Foundation of China (82101244 and 32170969), and Natural Science Foundation of Zhejiang Province, China (LY24C090006 and LY22H090002). **Author contributions:** M.Q. conceived and supervised the study. X.X. and M.Q. designed the experiments. X.X., M.F., and L.C. performed the experiments. H.H., Z.-M.D., and J.Y. provided unpublished reagents and analytical tools. X.X., M.F., and L.C. analyzed the data. X.X. wrote the first draft of the manuscript. X.X. and M.Q. revised the manuscript. **Competing interests:** The authors declare that they have no competing interests. **Data and materials availability:** All data needed to evaluate the conclusions in the paper are present in the paper and/or the Supplementary Materials. The RNA-seq datasets have been deposited in Gene Expression Omnibus (GEO): GSE253256. The Nzf2 ChIP-seq datasets have been deposited in Gene Expression Omnibus (GEO): GSE253254. The H3K9ac and H3K27 ChIP-seq datasets have been deposited in Gene Expression Omnibus (GEO): GSE253255. The ATAC-seq datasets have been deposited in Gene Expression Omnibus (GEO): GSE253491. They are publicly available as of the date of publication. All data are available in the main text or the Supplementary Materials. This study did not generate new unique reagents.

Submitted 28 May 2024
Accepted 7 November 2024
Published 13 December 2024
10.1126/sciadv.adf8405

Science Advances
AAAS

Supplementary Materials for

Nzf2 promotes oligodendrocyte differentiation and regeneration via repressing HDAC1-mediated histone deacetylation

Xiaofeng Xu *et al.*

Corresponding author: Mengsheng Qiu, msqiu@hznu.edu.cn

Sci. Adv. **10**, eadf8405 (2024)
DOI: 10.1126/sciadv.adf8405

The PDF file includes:

Figs. S1 to S7
Legends for tables S1 to S7

Other Supplementary Material for this manuscript includes the following:

Tables S1 to S7

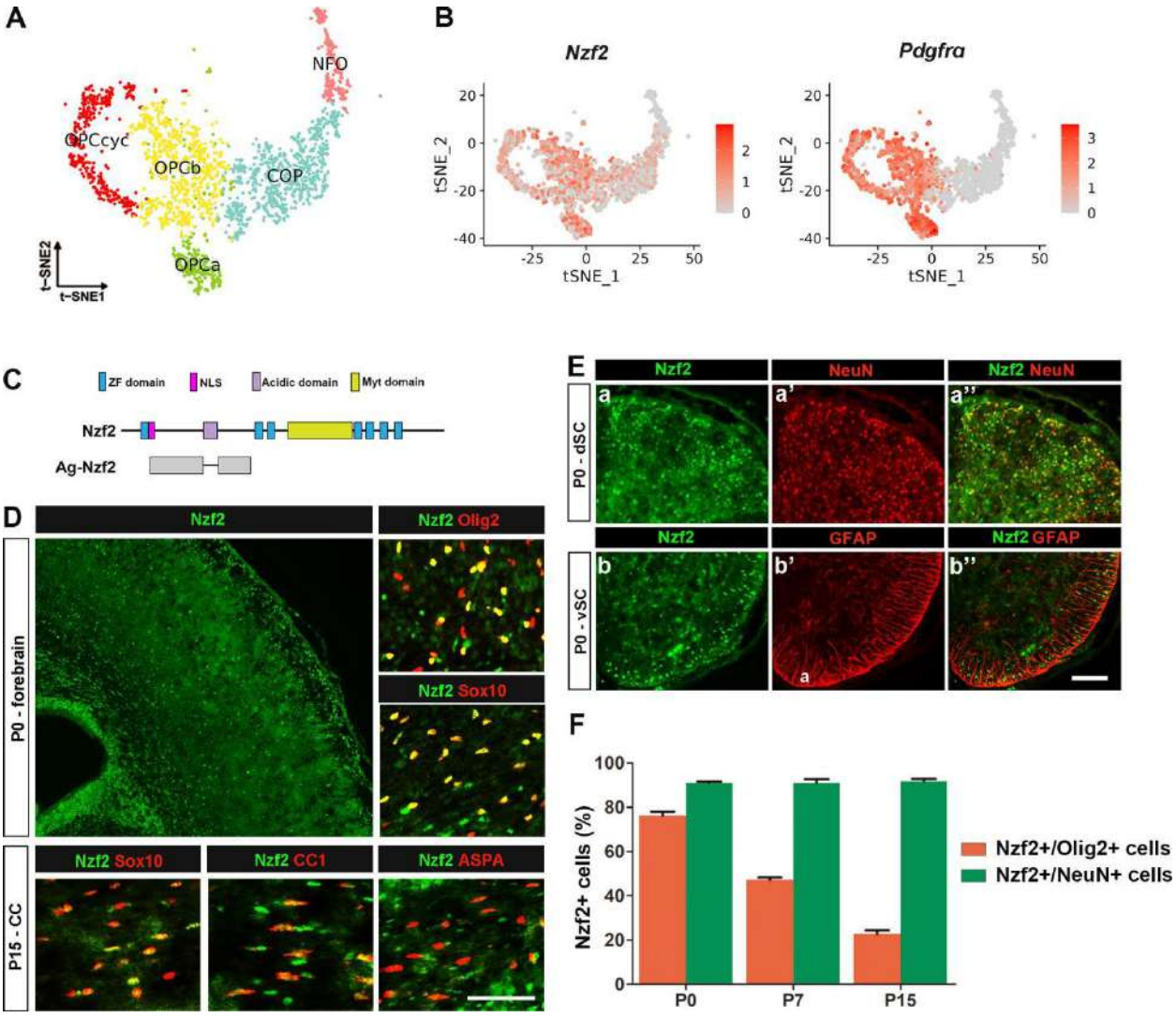

Fig. S1. Nzf2 is highly expressed in late OPCs and neurons in the CNS. (A) Sub-clustering analysis of OPCs and COPs as previously reported (*28*). **(B)** Representative transcription levels of *Nzf2* and *Pdgfra* in sub-clusters of OPCs and COPs. **(C)** Schematic diagram of the location of Nzf2-antigen peptides. **(D)** Double immunostaining of Nzf2 with different oligodendroglial markers (Olig2, Sox10, CC1 and ASPA) in the forebrain and corpus callosum (CC) of wild-type mice at P0 and P15, respectively. **(E)** Double immunostaining of Nzf2 with NeuN and GFAP in the spinal cords of wild-type mice at P0. **(F)** Quantification of the percentage of Nzf2/Olig2 double positive cells (orange) or Nzf2/NeuN double positive cells (green) among total Olig2 positive or NeuN positive cells in the spinal cords of wild-type mice at P0, P7 and P15, respectively. CC: corpus callosum. dSC: dorsal spinal cord. vSC: ventral spinal cord. Scale bar: 100 μm.

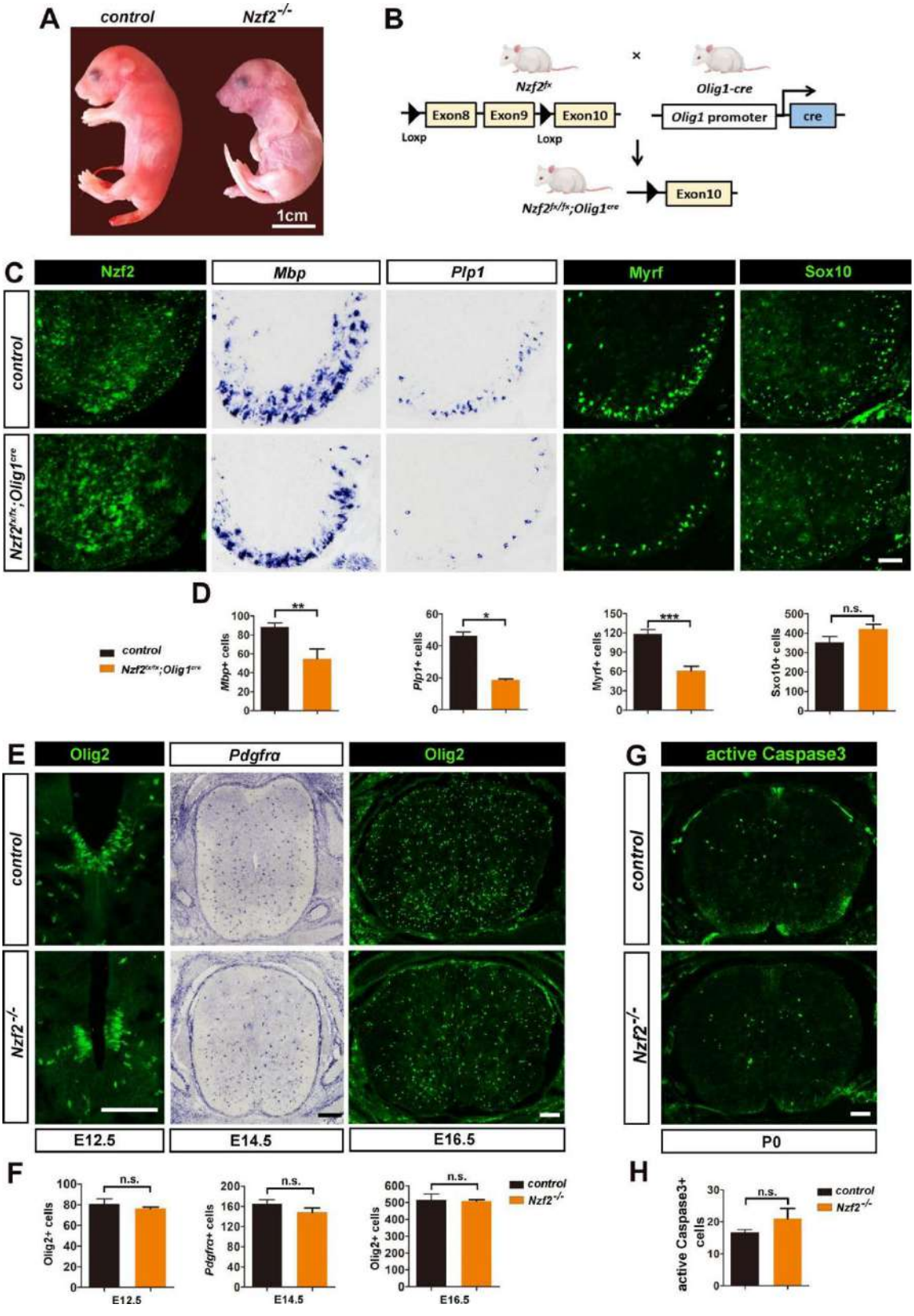
A
control
Nzf2-/-
1cm
B
Nzf2fx
Olig1-cre
Exon8
Exon9
Exon10
Loxp
Loxp
Olig1 promoter
cre
Nzf2fx/fx;Olig1cre
Exon10
C
Nzf2
Mbp
Plp1
Myrf
Sox10
control
Nzf2fx/fx;Olig1cre
D
control
Nzf2fx/fx;Olig1cre
Mbp+ cells
Plp1+ cells
Myrf+ cells
Sxo10+ cells
**
*
***
n.s.
E
Olig2
Pdgfrα
Olig2
control
Nzf2-/-
E12.5
E14.5
E16.5
G
active Caspase3
control
Nzf2-/-
P0
F
Olig2+ cells
Pdgfrα+ cells
Olig2+ cells
n.s.
control
Nzf2-/-
E12.5
E14.5
E16.5
H
active Caspase3+ cells
n.s.
control
Nzf2-/-

Fig. S2. **Conditional knockout of *Nzf2* resulted in a dramatic delay in OL differentiation. (A)** Phenotypes of control and *Nzf2*$^{-/-}$ mouse at P0. *Nzf2*$^{-/-}$ mice died neonatally without apparent deficiency. **(B)** Schematic representation of the generation of *Nzf2* cKO mice. (C) Immunostaining of Nzf2, Myrf and Sox10, ISH of *Mbp* and *Plp1* in the spinal cords of control and *Nzf2* cKO mice at P3. (D) Quantification of *Mbp*+, *Plp1*+, Myrf+ and Sox10+cells per section in the spinal cords of control and *Nzf2* cKO mice at P3 from (B). **(E)** Immunostaining of Olig2 and ISH of *Pdgfrα* in the spinal cords of control and *Nzf2*$^{-/-}$ mice at E12.5, E14.5 and E16.5. **(F)** Quantification of Olig2 positive and *Pdgfrα* positive cells per section in the spinal cords of control and *Nzf2*$^{-/-}$ mice at E12.5, E14.5 and E16.5 from (D). **(G)** Immunostaining of active Caspase 3 in the spinal cords of control and *Nzf2*$^{-/-}$ mice at P0. **(H)** Quantification of active Caspase 3 positive cells per section in the spinal cords of control and *Nzf2*$^{-/-}$ mice at P0 from (F). Error bars indicated *SEM*. *$p \leq 0.01$, **$p \leq 0.005$, ***$p \leq 0.001$. n.s.: no significant difference. Scale bar: 100 μm.

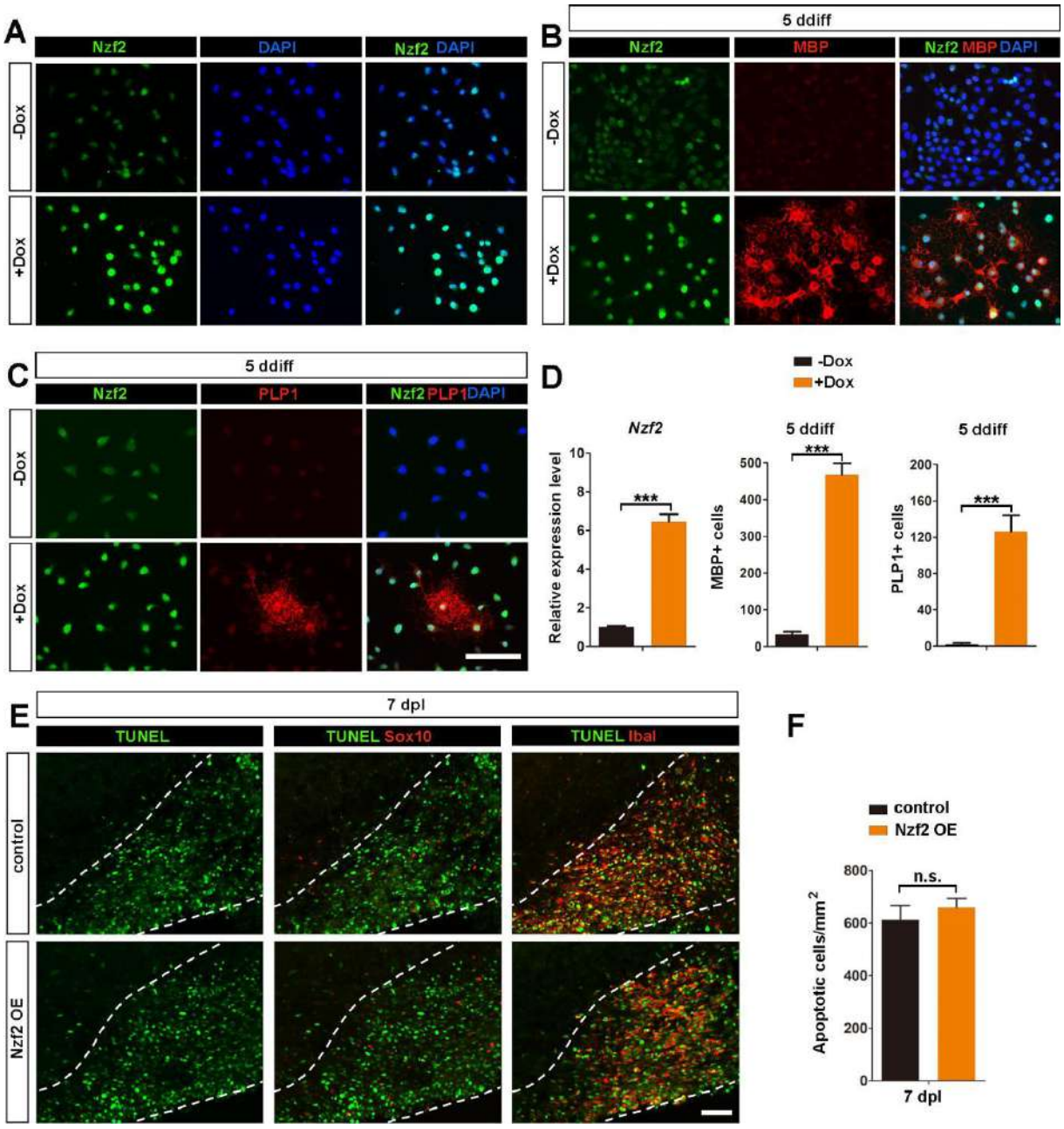

Fig. S3. Hyperactivation of Nzf2 induces precocious OL differentiation. (A) Immunostaining of Nzf2 in CG4 in the proliferation medium with or without Dox treatment. Nuclei were stained with DAPI. **(B)** Double immunostaining of Nzf2 (green) and MBP (red) in CG4 cells in the differentiation medium with or without Dox treatment at 5 ddiff. Nuclei were stained with DAPI. **(C)** Double immunostaining of Nzf2 (green) and PLP1 (red) in CG4 cells in the differentiation medium with or without Dox treatment at 5 ddiff. Nuclei were stained with DAPI. **(D)** Quantification of *Nzf2* expression levels, MBP+ and PLP1+ cells per dish in CG4 cells with or without Dox treatment from (A), (B) and (C). **(E)** TUNEL assays and co-staining with Sox10 and Iba1 in control-virus and Nzf2-virus injected injury areas at 7 dpl. **(F)** Quantification of apoptotic cells (calculated per mm^2) at 7 dpl from (E). Error bars indicated *SEM*. ***$p \leq 0.001$. n.s.: no significant difference. Scale bar: 100 μm.

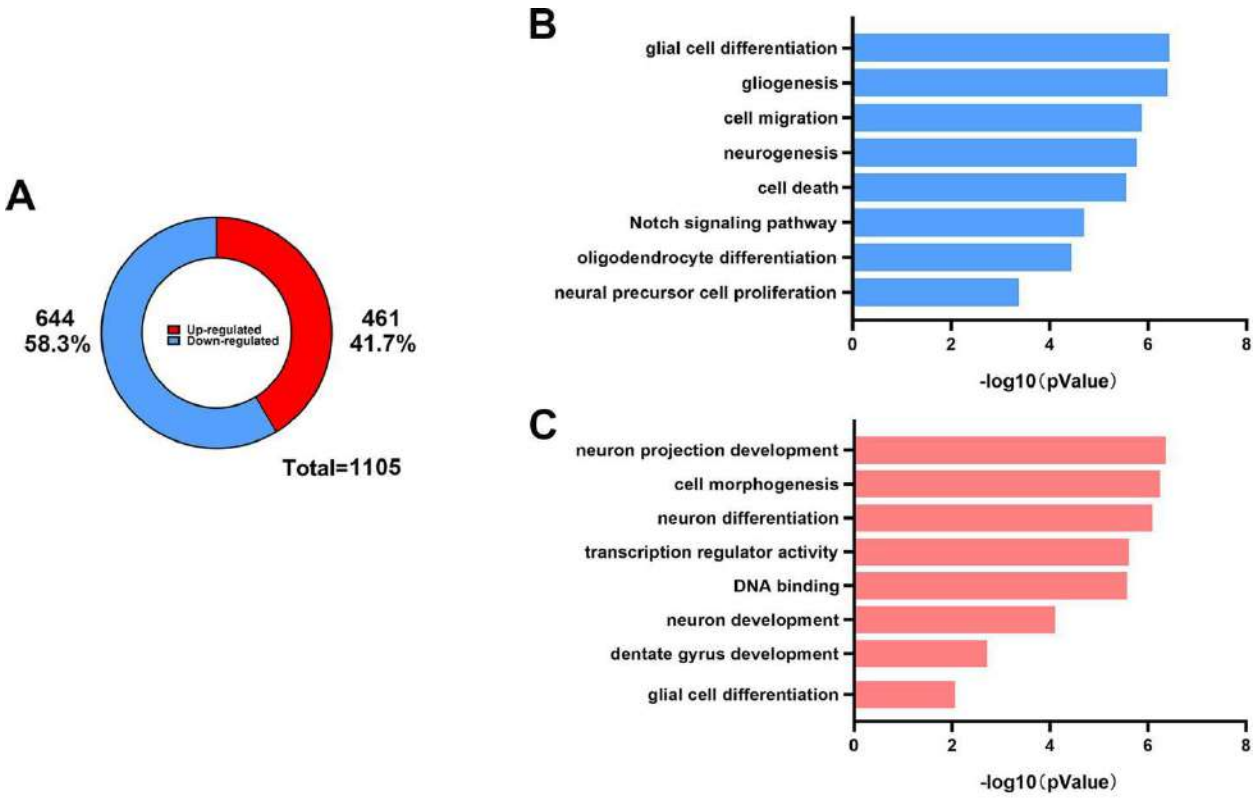

Fig. S4. Gene ontology analysis of differentially expressed genes after *Nzf2* deletion. (A) Pie chart of the percentage of differentially expressed genes between wild-type and *Nzf2*$^{-/-}$ spinal cords at P0. **(B)** Gene ontology (GO) analysis of the significantly down-regulated genes in the spinal cords of *Nzf2*$^{-/-}$ mice at P0, compared to that in wild-type mice. **(C)** Gene ontology (GO) analysis of the significantly up-regulated genes in the spinal cords of *Nzf2*$^{-/-}$ mice at P0, compared to that in wild-type mice.

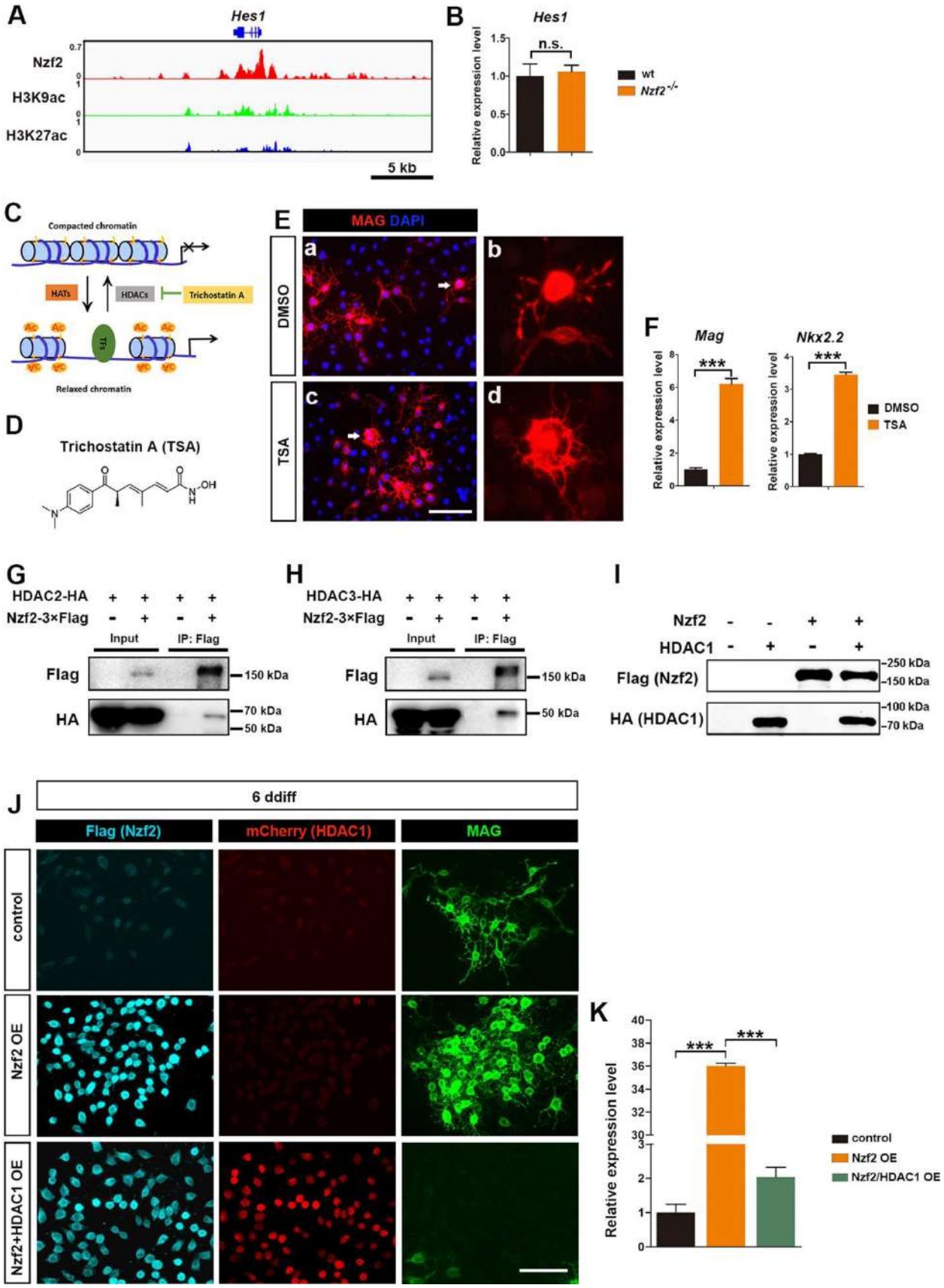
A
Hes1
Nzf2
H3K9ac
H3K27ac
5 kb
B
Hes1
n.s.
Relative expression level
wt
Nzf2 -/-
C
Compacted chromatin
HATs
HDACs
Trichostatin A
TFs
Relaxed chromatin
D
Trichostatin A (TSA)
E
MAG DAPI
DMSO
TSA
a
b
c
d
F
Mag
Nkx2.2
***
Relative expression level
DMSO
TSA
G
HDAC2-HA
Nzf2-3×Flag
Input
IP: Flag
Flag
HA
150 kDa
70 kDa
50 kDa
H
HDAC3-HA
Nzf2-3×Flag
Input
IP: Flag
Flag
HA
150 kDa
50 kDa
I
Nzf2
HDAC1
Flag (Nzf2)
HA (HDAC1)
250 kDa
150 kDa
100 kDa
70 kDa
J
6 ddiff
Flag (Nzf2)
mCherry (HDAC1)
MAG
control
Nzf2 OE
Nzf2+HDAC1 OE
K
***
***
Relative expression level
control
Nzf2 OE
Nzf2/HDAC1 OE

Fig. S5. Nzf2 regulates target gene expression via physical interaction with HDAC1. (A) The enrichment of Nzf2 at *Hes1* gene loci, which was not modified by H3K9ac or H3K27ac. **(B)** qRT-PCR analysis of *Hes1* expression levels in the spinal cords of wild-type and *Nzf2*$^{-/-}$ mice at P0. **(C)** Schematic diagram of the histone acetylation balance mediated by HATs and HDACs, and HDAC inhibitor, TSA. **(D)** The chemical formula of TSA. **(E)** Immunostaining of MAG (red) in CG4 cells at 6 ddiff with or without TSA treatment. The right panels are the magnified images of cells pointed by arrows. **(F)** qRT-PCR analysis of *Mag* and *Nkx2.2* in CG4 cells at 6 ddiff with or without TSA treatment. **(G and H)** Co-IP analysis of HDAC2-HA or HDAC3-HA with Nzf2-3×Flag from transiently transfected HEK293T cells. **(I)** Western blot analysis confirmed the overexpression of Nzf2 and HDAC1, respectively. **(J)** Triple immunostaining of Nzf2-Flag (blue), HDAC1 (red) and MAG (green) in control, Nzf2-overexpressed, Nzf2 and HDAC1 co-overexpressed CG4 cells at 6 ddiff. **(K)** qRT-PCR analysis of *Mag* expression levels in control, Nzf2-overexpressed, Nzf2 and HDAC1 co-overexpressed CG4 cells at 6 ddiff from (J). Errors bars indicated *SEM*. ***p*≤0.005, ****p*≤0.001, n.s.: no significant difference. Scale bar: 100 μm.

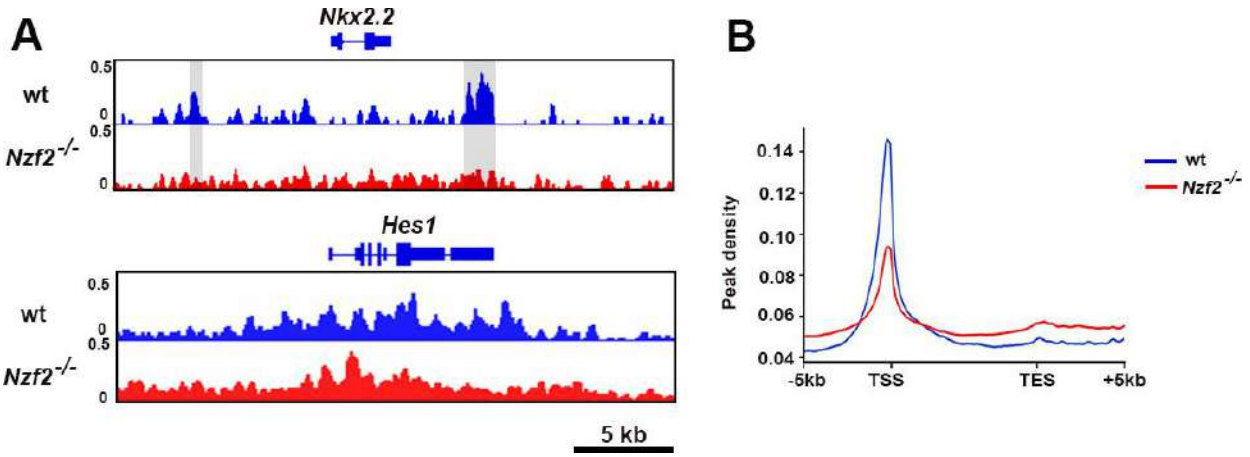

Fig. S6. Nzf2 establishes an accessible chromatin landscape to promote downstream gene transcription. (A) Representative ATAC-seq tracks of *Nkx2.2* and *Hes1* in wild type and *Nzf2* KO mice. **(B)** Distribution of ATAC-seq peaks around TSS in wild type and *Nzf2* KO mice.

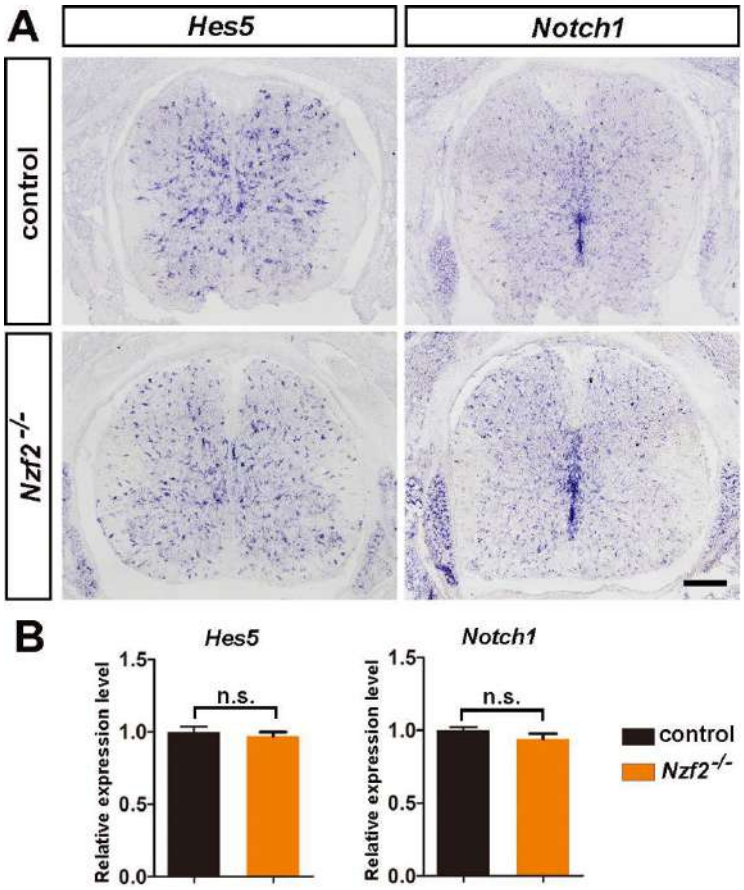

Fig. S7. Deletion of Nzf2 does not affect the expression of Notch signaling target genes. (A) ISH of *Hes5* and *Notch1* in the spinal cords of wild-type and *Nzf2*$^{-/-}$ mice at P0. **(B)** qRT-PCR analysis of *Hes5* and *Notch1* expression levels in the spinal cords of wild-type and *Nzf2*$^{-/-}$ mice at P0. Error bars indicated *SEM*. n.s.: no significant difference. Scale bar: 100 μm.

Table S1. Differentially expressed genes identified by RNA-seq.xlsx

Table S2. Nzf2 target genes identified by Nzf2 ChIP-seq.xlsx

Table S3. Nzf2 direct target gene list.xlsx

Table S4. Different peak-related genes identified by ATAC-seq (Nzf2 ko vs wt).xlsx

Table S5. Genotyping primers.xlsx

Table S6. Antibodies used in this study.xlsx

Table S7. Real-time PCR primers and ChIP-qPCR primers.xlsx